


## Article

# Simulation-Based Optimization Workflow of CO<sub>2</sub>-EOR for Hydraulic Fractured Wells in Wolfcamp A Formation

Dung Bui <sup>1,\*</sup> , Duc Pham <sup>1</sup> , Son Nguyen <sup>2</sup> and Kien Nguyen <sup>3</sup>

<sup>1</sup> New Mexico Institute of Mining and Technology, 801 Leroy Place, Socorro, NM 87801, USA; duc.pham@student.nmt.edu

<sup>2</sup> Department of Petroleum Engineering, University of Houston, Houston, TX 77023, USA; stnguyen64@uh.edu

<sup>3</sup> Office of Institutional Research, The University of North Carolina at Pembroke, Pembroke, NC 28372, USA; kien29101996@gmail.com

\* Correspondence: dung.bui@nmt.edu

**Abstract:** Hydraulic fracturing has enabled production from unconventional reservoirs in the U.S., but production rates often decline sharply, limiting recovery factors to under 10%. This study proposes an optimization workflow for the CO<sub>2</sub> huff-n-puff process for multistage-fractured horizontal wells in the Wolfcamp A formation in the Delaware Basin. The potential for enhanced oil recovery and CO<sub>2</sub> sequestration simultaneously was addressed using a coupled geomechanics–reservoir simulation. Geomechanical properties were derived from a 1D mechanical earth model and integrated into reservoir simulation to replicate hydraulic fracture geometries. The fracture model was validated using a robust production history matching. A fluid phase behavior analysis refined the equation of state, and 1D slim tube simulations determined a minimum miscibility pressure of 4300 psi for CO<sub>2</sub> injection. After the primary production phase, various CO<sub>2</sub> injection rates were tested from 1 to 25 MMSCFD/well, resulting in incremental oil recovery ranging from 6.3% to 69.3%. Different injection, soaking and production cycles were analyzed to determine the ideal operating condition. The optimal scenario improved cumulative oil recovery by 68.8% while keeping the highest CO<sub>2</sub> storage efficiency. The simulation approach proposed by this study provides a comprehensive and systematic workflow for evaluating and optimizing CO<sub>2</sub> huff-n-puff in hydraulically fractured wells, enhancing the recovery factor of unconventional reservoirs.



**Citation:** Bui, D.; Pham, D.; Nguyen, S.; Nguyen, K. Simulation-Based Optimization Workflow of CO<sub>2</sub>-EOR for Hydraulic Fractured Wells in Wolfcamp A Formation. *Fuels* **2024**, *5*, 673–697. <https://doi.org/10.3390/fuels5040037>

Academic Editor: Martin Olazar

Received: 13 July 2024

Revised: 1 September 2024

Accepted: 16 October 2024

Published: 18 October 2024



**Copyright:** © 2024 by the authors. Licensee MDPI, Basel, Switzerland. This article is an open access article distributed under the terms and conditions of the Creative Commons Attribution (CC BY) license (<https://creativecommons.org/licenses/by/4.0/>).

**Keywords:** CO<sub>2</sub>-EOR huff-n-puff; hydraulic fracturing simulation; hydrodynamic–geomechanical coupled model; Wolfcamp A formation; optimizing recovery of unconventional reservoir

## 1. Introduction

Oil and natural gas production from unconventional reservoirs with ultra-low permeability constitutes the majority of petroleum production in the United States, with 64% of crude oil produced in 2023 from tight-oil formations [1]. In order to overcome the low permeability nature of these reservoirs, horizontal wells with multi-stage hydraulic fracturing are employed as standard industry practice. The production of these wells, however, usually suffers a sharp decline after the first few years [2,3]. This phenomenon results from formation damage due to a wide range of mechanisms: invasion of high-pressure fracturing fluids [4], proppant embedment, gel filter cake and gel residue [5], formation of biofilm inside fractures [6] and fracture choking from deposition of asphaltene [7]. In addition, more intensive and frequent hydraulic fracturing in the same play can result in a steeper production decline and result in lower recovery [8]. To improve oil recovery, a popular stimulation technique employed by operators is CO<sub>2</sub> huff-and-puff. This is considered the most effective oil recovery method based on CO<sub>2</sub> injection [9]. The procedure involves two phases: CO<sub>2</sub> injection (huff) and soaking (puff). In the huff phase, immiscible CO<sub>2</sub> is injected at high pressure into the reservoir to increase pressure and push oil toward production wells [10]. Afterward, the reservoir rests in the puff phase so that the injected

CO<sub>2</sub> can mix with the oil, causing it to swell and reducing its viscosity [11] and oil–water interfacial tension [12]. The light hydrocarbon components of the crude oil will be extracted by the dissolved CO<sub>2</sub> [13]. Production then resumed after the soaking period with an improved rate due to lower viscosity and CO<sub>2</sub> expansion displacing the oil [14]. CO<sub>2</sub> huff-n-puff depends on some major mechanisms such as viscosity reduction [15], interfacial tension reduction and oil swelling [16]. It is a well-established, highly applicable and cost-effective enhanced oil recovery (EOR) method that provides a substantial increase in oil recovery [17,18]. In addition, it brings environmental benefits by reducing the amount of CO<sub>2</sub> released into the atmosphere. Operators can also enjoy 45Q tax credits from CO<sub>2</sub> storage [19].

Studies on CO<sub>2</sub> huff-n-puff have been focused on a numerical simulation approach instead of mathematical modeling [9]. There have been numerous works attempting to simulate and optimize the huff-n-puff process by changing operating parameters like injection time and volume, soaking time and injection pressure [20]. Afari et al. [21] combined compositional reservoir simulation and response surface methodology (RSM) to investigate the impact of operating parameters and concluded that production bottom hole pressure and period were critical in determining oil recovery, while injection rate and periods were much less influential. Song and Yang [22] performed a numerical simulation with multiple wells and heterogeneous reservoirs to evaluate huff-n-puff performance in the Bakken formation and optimize the injection pressure, soaking time and production pressure. Sensitivity analysis showed that higher injection pressure and lower wellhead pressure could lead to higher oil recovery, though the effect was only noticeable around the wellbore. The optimal soaking time was determined to be 15 days. Zhou et al. [23] attempted to optimize optimized pressure depletion and injection rate through an experimental and mathematical study. The authors noted improvement in recovery factor as injection pressure increased and then calculated the optimal pressure depletion rate to be 4 kPA/min. Sheng [24] developed a numerical model to optimize huff time, puff time and soaking time for huff-n-puff in a shale oil reservoir. Based on the study, the author concluded that huff time should be set as long as possible while soaking time could even be eliminated. This is fundamentally different from many field tests and laboratory tests [25]. The conclusion, however, can be challenged due to the model having few blocks (11 × 31 × 1), hence not being refined enough to fully capture the heterogeneity and variance along the z-direction of the reservoir. Wang et al. [26] studied the impact of primary depletion time, injection time, cycle number, production time and CO<sub>2</sub> injection rate on cumulative oil production and net present value using response surface methodology (RSM). Analysis was performed on a finely-gridded, homogeneous numerical simulation. Results showed that cumulative oil production could be modeled as a quadratic function of the aforementioned parameters. The study provided an effective approach to the optimization of operating parameters. Nevertheless, the numerical model was homogenous, with only one multistage fractured horizontal well, which raised concerns about its applicability to more complicated scenarios. Hao et al. [27] performed a sensitivity analysis of both reservoir and operating parameters to optimize the oil production rate through experimental tests and numerical simulation. Cumulative CO<sub>2</sub> injection rate was determined to be the most influential operating parameter. Similar to Wang et al. [26], the numerical model was homogenous, with a single well at the center and a perfect planar fracture.

While providing important insights, to date, no research has comprehensively captured the CO<sub>2</sub> huff-n-puff process. Most papers assume a homogeneous reservoir with a single horizontal well, even though reservoir heterogeneity has a significant impact on the effectiveness of huff-n-puff [28]. As an exception, with a non-homogenous reservoir, the study of Song and Yang [22] did not simulate the hydraulic fracturing process and relied on field data to create uniform fractures, hence not fully taking into account geomechanical properties. All of these limitations reduce the rigorousness and applicability of the models. There arises the need for a more thorough workflow that covers all aspects of the huff-n-puff operation, from data collection and model development to optimization.

This paper introduces a pioneering optimization workflow of CO<sub>2</sub> huff-n-puff through dynamic numerical simulation and sensitivity analysis approach, using data from two adjacent horizontal hydraulic fracture wells in Wolfcamp A formation in the Delaware Basin. All reservoir, fluid and fracture properties were calculated based on log and historical production data. The fracture geometry of these two wells was accurately simulated using a finely-gridded, integrated geomechanics–hydrodynamic compositional reservoir simulation and validated using fracture treatment data and performing production history matching. Due to its comprehensiveness, this workflow eliminates the need to make assumptions about reservoir or fracture properties and can be applied to huff-n-puff optimization in any reservoir and formation.

## 2. Materials and Methods

### 2.1. Methodology

A fully-coupled geomechanics–hydrodynamic model was designed to simulate the growth of fractures during hydraulic fracturing and optimize the CO<sub>2</sub> huff-n-puff process to maximize oil recovery. Initially, the simulation involved integrating geomechanical properties with a dual permeability model using a compositional simulator commonly used by the oil and gas industry. The integrated model is capable of replicating hydraulic fracture geometries employing fracture treatment data from the field. The model implements the following two sets of fundamental equations: one for the fluid flow within a porous medium and another for the deformation of the rock. The fluid flow equations include conservation of mass and Darcy’s law [29]; the basic equations for rock deformation comprise the constitutive law of deformation, strain and stress. The fluid flow equation in the porous medium is expressed as follows [30]:

$$\frac{\partial}{\partial t} (\phi^* \rho_f) - \nabla \cdot \left( \rho_f \frac{\mathbf{k}}{\mu} [\nabla p - \rho_f \mathbf{g}] \right) = Q_f \quad (1)$$

where  $\phi^*$  is reservoir porosity;  $\rho_f$  is the fluid density, kg/m<sup>3</sup>;  $Q_f$  is the mass flow rate of fluid per unit volume;  $\mathbf{k}$  is absolute permeability tensor, m<sup>2</sup>;  $p$  is fluid pressure, Pa;  $\mathbf{g}$  is gravitational acceleration, m/s<sup>2</sup>;  $\mu$  is fluid viscosity, Pa.s.

The government equation for the geomechanics module can be expressed as follows:

$$\nabla \cdot \left[ \mathbf{C} : \frac{1}{2} (\nabla \mathbf{u} + (\nabla \mathbf{u})^T) \right] = \rho_r \mathbf{B} - \nabla \cdot (\alpha p) \mathbf{I} \quad (2)$$

where  $\mathbf{C}$  is the tangential stiffness tensor;  $\mathbf{u}$  is the displacement vector;  $\rho_r$  is solid grain density, kg/m<sup>3</sup>;  $\mathbf{B}$  is the body force acting throughout a unit volume;  $\alpha$  is Biot’s constant;  $p$  is fluid pressure;  $\mathbf{I}$  is unit tensor.

The iterative coupled approach is employed to solve the fluid flow and rock deformation equations. This approach is chosen for its reliability and efficiency [31]. The steps involved in the iterative coupling technique are as follows: (1) Initial pressure is calculated using the reservoir flow simulator at a specified timestep; (2) pressure is transmitted to the geomechanics simulator to calculate displacement, strain and stress; (3) reservoir porosity, influenced by pressure and stress, is updated using volumetric strain. The updated porosity is used to recompute reservoir pressure. (4) The recalculated pressure is sent back to the geomechanics simulator for updated deformation calculations. The process iterates until a predetermined tolerance is achieved [6,32]. The iterative coupling approach is depicted in Figure 1, providing a concise summary of its diagram.

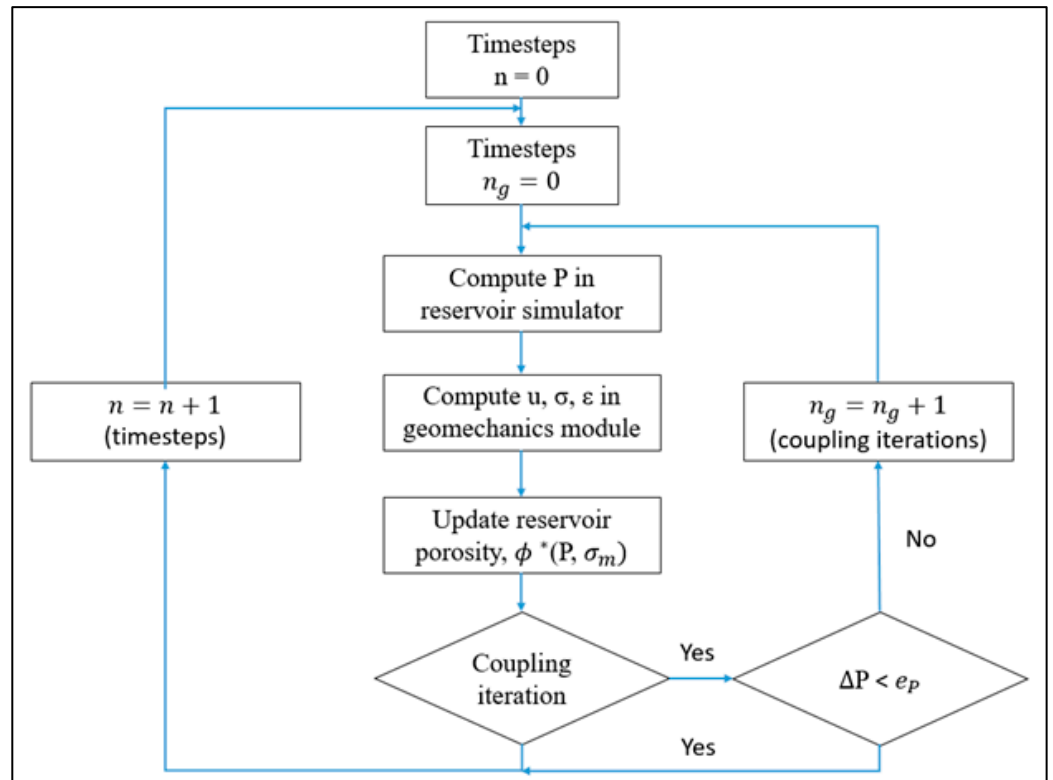


Figure 1. Generalized flow diagram for iterative coupling [33].

2.1.1. Modeling of Hydraulic Fracture’s Permeability

The modified Barton–Bandis model (1983) [34] is used to determine fracture permeability based on closure stress. The hydraulic fracturing process is described (Figure 2) as follows:

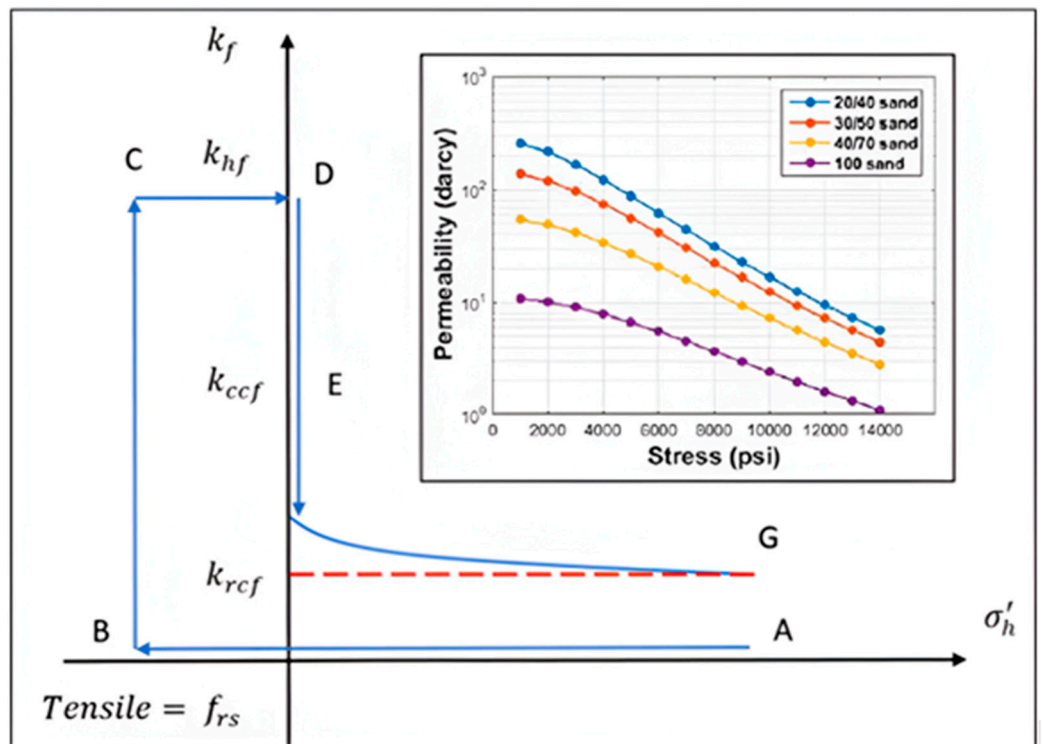


Figure 2. Modified Barton–Bandis fracture permeability model [30,34].



Fracture Initiation: Initial equilibrium state at point A with effective minimum horizontal stress ( $\sigma_h'$ ). Elevated injection rate and pressure increase pore pressure, reducing  $\sigma_h'$  from point A to point B. Fracture initiation at point B when  $\sigma_h'$  drops to tensile strength ( $f_{rs}$ ). The fracture permeability ( $k_{hf}$ ) in the stimulated zone is at the maximum value and equal to the intrinsic permeability of the proppant.

Fracture Closure: As stress increases from point C to point D, permeability decreases from  $k_{hf}$  to closure permeability ( $k_{ccf}$ ). Closure stress acting on fractures supported by proppant gradually reduces fracture permeability to residual fracture permeability ( $k_{rcf}$ ). The blue arrows follow the path of ABCDEG, illustrating the behavior of fractures from their initiation to maximum opening, and finally to closure. The red dashed line shows the residual fracture permeability at closure, representing the long-term permeability supported by proppant particles.

### 2.1.2. CO<sub>2</sub> Huff-n-Puff Development

After primary recovery, a field-scale development is implemented to evaluate different injection scenarios and optimize CO<sub>2</sub> huff-n-puff in two depleted fractured horizontal wells. The following four steps generated a detailed optimization workflow for CO<sub>2</sub>-enhanced oil recovery (CO<sub>2</sub>-EOR) application in the field.

#### Fluid Model Generation:

The dynamic reservoir simulation modeling begins with generating an equation of state (EOS) fluid model. The compositional reservoir fluid model was fine-tuned to an equation of state using the 3-parameter Peng Robinson model. The laboratory test and analysis performed on the reservoir fluid yielded several components, with the plus fraction beginning from C30. The fluid components were lumped into the seven components to reduce the computational overload [35]. The fluid viscosity was modeled using the Jossi–Stiel–Thodos (JST) correlation. PVT tuning was performed by identifying sensitive fluid properties and regressing them to obtain acceptable matches with the laboratory data. Among the parameters, the critical temperatures, critical pressures and molecular weights of the fluid components heavily impacted the regression.

#### Slim Tube Simulation Test:

The minimum miscibility pressure (MMP) can be measured accurately with experimental methods in the laboratory. However, these experimental methods are very costly and time-consuming [36]. Therefore, after the PVT tuning, a 1D slim tube test using compositional reservoir simulation was performed to estimate the MMP. Generally, purchased and recycled CO<sub>2</sub> contain impurities that are likely to impact the MMP. Impurities were introduced to the fluid in increments to model real-life impact on CO<sub>2</sub>-EOR performance.

#### History Matching:

After hydraulic fracturing, the two investigated wells have been producing for about five years and are still active. To verify the quality of the fracture model, several techniques can be deployed, including but not limited to monitoring techniques, post-fractured production analysis [33,37–39], treatment pressure matching for injection periods and production and flowing bottom hole pressure (BHP) matching for the production phase. In this study, the two wells' production and flowing bottom hole pressure are available, so they were used as the primary references for validation. Among the above uncertain parameters, reservoir properties, matrix relative permeability curves and operating conditions are either calculated from log data and calibrated using published data or obtained from well historical data. Since there are two horizontal hydraulic fracture wells modeled, the history-matching process in this research is iterative, as demonstrated in Figure 3. The blue arrows in Figure 3 illustrate the step-by-step history matching process, while the green arrows indicate where matching parameters need to be updated until convergence is achieved.

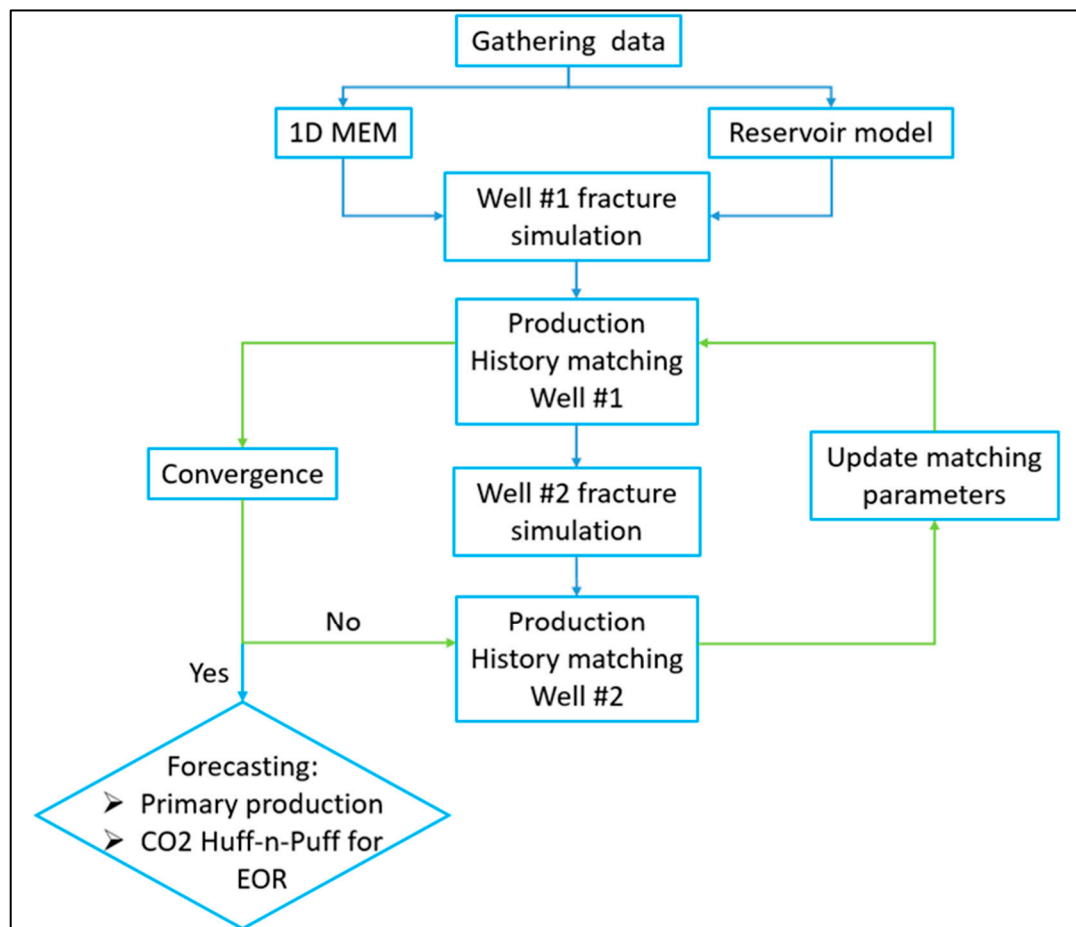


**Figure 3.** Iterative history matching process for fracture model's validation.

#### Field development evaluation:

A comprehensive simulation analysis was conducted to optimize the CO<sub>2</sub> huff-n-puff process for CO<sub>2</sub>-EOR. The study investigated various CO<sub>2</sub> injection rates along with different injecting, soaking and producing time ratios. Several combinations of cycle times were analyzed to determine the optimal cycle. Based on the simulation results, the optimal operating conditions for CO<sub>2</sub>-EOR in the unconventional Wolfcamp A formation in the Delaware Basin were identified.

Combining a dual permeability model and geomechanical module in a compositional simulation provided a robust framework for optimizing CO<sub>2</sub> huff-n-puff injection in depleted horizontal fractured wells.

#### 2.2. Geological Description and Properties

The Wolfcamp formation, which was formed from the late Pennsylvanian to the end of the Wolfcampian period, extends over all of the Permian Basin. The Wolfcamp formation is an intricate geological unit mostly composed of shale with high organic content and intervals of carbonate rocks that include clay minerals [40]. The sub-basins, including the Delaware Basin, Central Basin Platform, and Midland Basin, exhibit substantial variations in depth, thickness and lithology. The heterogeneity of this formation is governed by depositional and diagenetic mechanisms. From a stratigraphic perspective, the Wolfcamp formation consists of four stratified intervals labeled as the A, B, C and D sequences, as shown in Figure 4.

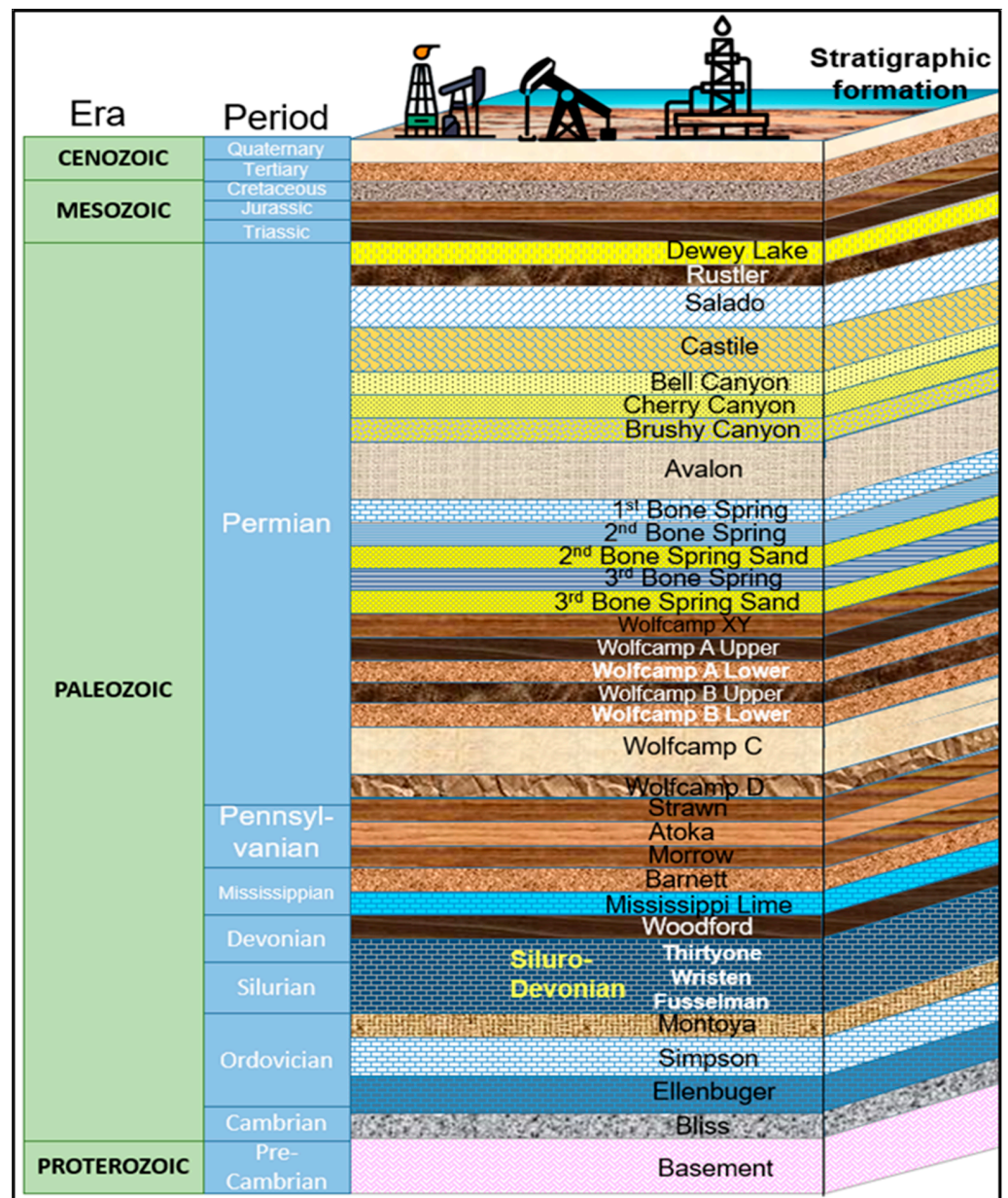


Figure 4. Schematic stratigraphy of Wolfcamp formation [41].

The majority of the present drilling operations in the Delaware and Midland Basins are focused on the Upper Wolfcamp, named the A and B formations. These layers are characterized by a higher abundance of natural gas and more mature phases of hydrocarbon yield compared to the Lower Wolfcamp C and D reservoirs [42]. On top of that, the Wolfcamp A formation consists of alternating layers of shale, siltstone, sandstone and carbonate rocks (Figure 5). The thin interbeds of sandstones and limestones within the shales can act as storage units for hydrocarbons. However, the tight nature of these rocks makes it difficult to conventionally extract oil and gas from them.

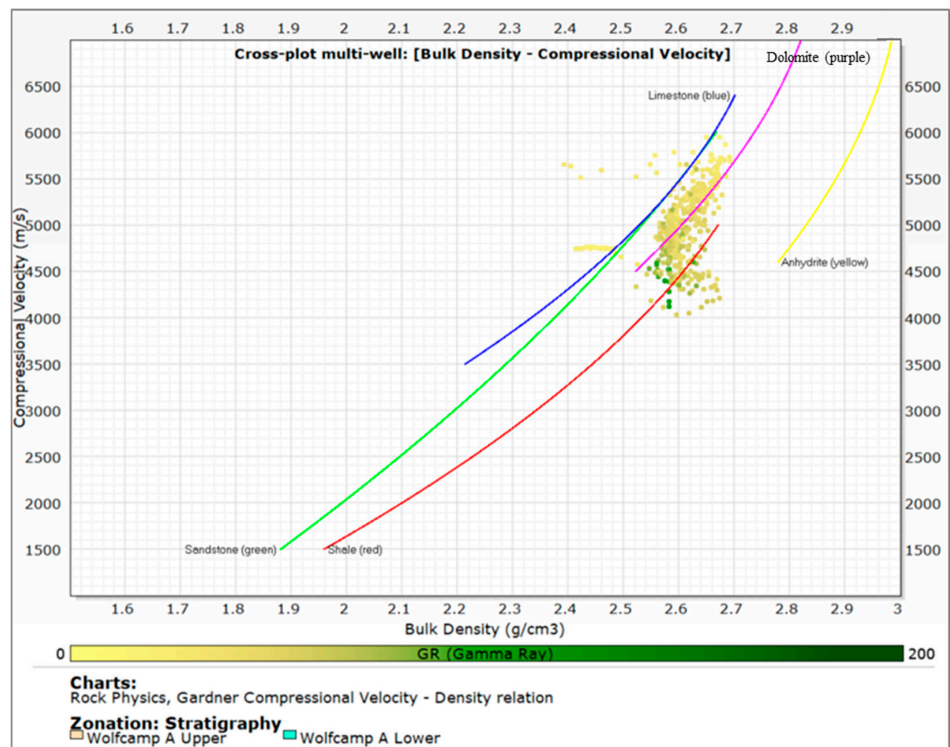


Figure 5. Lithological characteristic of the Wolfcamp A formation.

In a recent paper, Bui et al. [43] constructed a detailed methodology and equations to estimate the petrophysical parameters and develop a 1D mechanical earth model for the Third Bonespring Sand in the Delaware basin. This study continues to use the same approach and formulas to calculate essential petrophysical elements for the Wolfcamp A formation at Lea County, such as shale volume and total and effective porosities. The findings show that the average shale volume is about 55%, the average total porosity is 0.09 and the effective porosity is 0.05 (Figure 6).

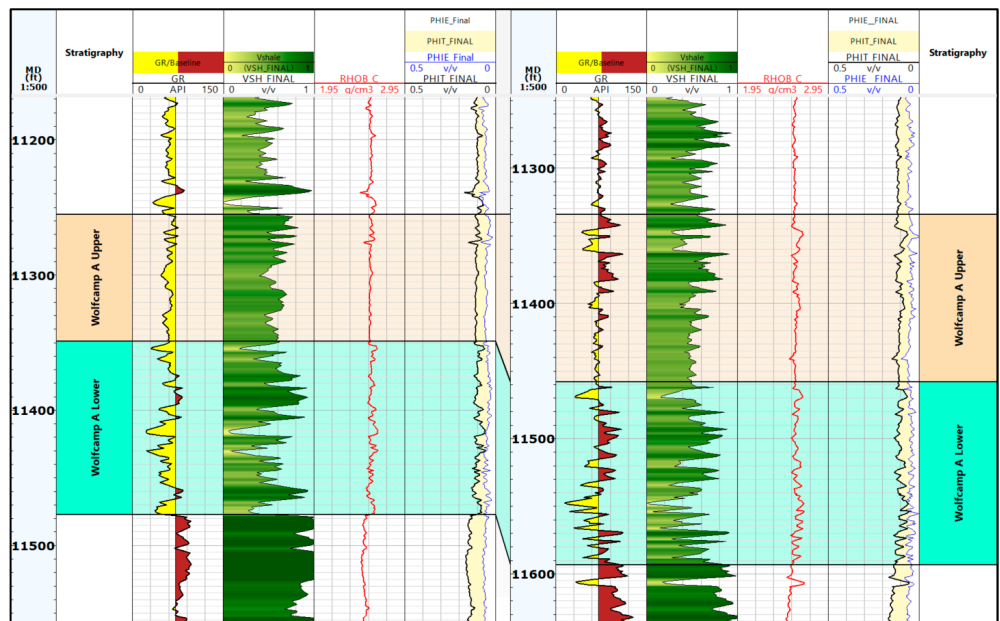


Figure 6. Petrophysical interpretation of Wolfcamp A formation in the offset wells.



From the perspective of the in situ stresses, the developed 1D geomechanical model illustrates that the pore pressure gradient increases from 0.6 psi/ft at the top of the Wolfcamp A formation to a peak of 0.7 psi/ft. The minimum and maximum horizontal stresses are characterized by pressure gradients of 0.79 psi/ft and 0.87 psi/ft, respectively. In addition, the vertical stress indicates a pressure gradient of 1.1 psi/ft (Figure 7).

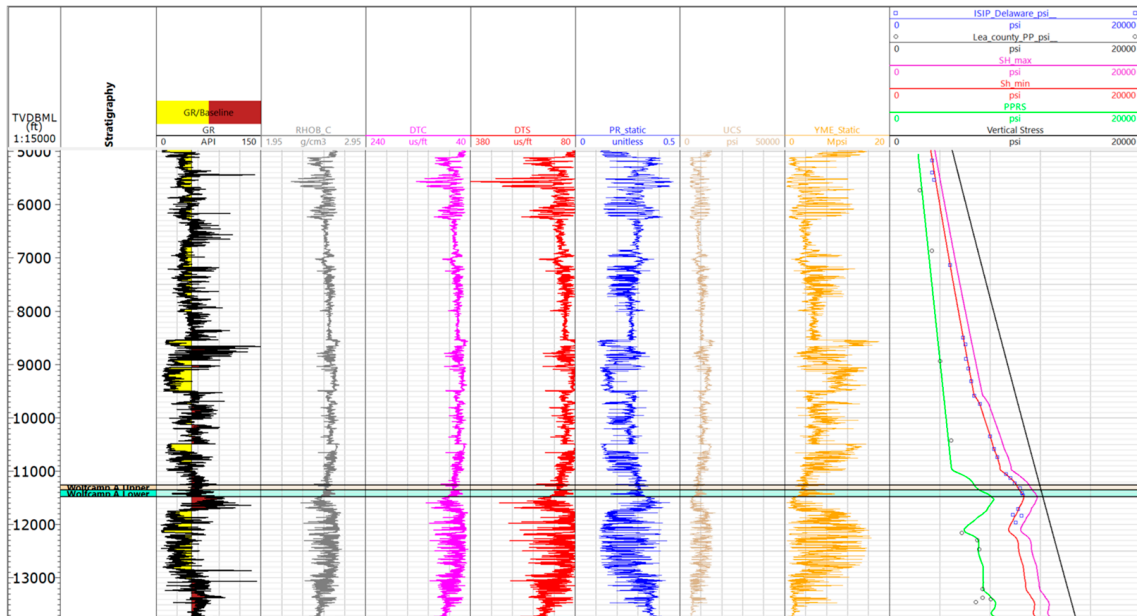


Figure 7. 1D geomechanical model for the Wolfcamp A formation.

The rock properties are essential in representing the mechanical behavior of the reservoir [44], which is critical for hydraulic fracturing simulation. The statistical data pertaining to the Wolfcamp A formation in Figure 8 display average values of 4.2 Mpsi for static Young’s modulus, 0.29 for static Poisson ratio and 8854 psi for unconfined compressive strength (UCS).

### 2.3. Simulation Setup

The numerical model employed for this study was a dual-permeability model, which was developed using the Computer Modelling Group (CMG)—GEM reservoir simulator. This widely accepted simulator allows for the detailed representation and simulation of fluid flow and other geomechanics–hydrodynamic behaviors. The entire reservoir is discretized into  $103 \times 101 \times 6$  grid blocks in the x, y and z directions, with total lengths in x- and y-direction of 5150 ft and 2500 ft, respectively. The vertical extent of the reservoir, from top to bottom, ranges from 11,300 feet to 11,500 feet below the surface, giving an average formation thickness of 250 feet. This detailed grid setup deployed formation tops and well logs of four nearby vertical wells in the Wolfcamp A formation, allowing a precise simulation of the field operations. A summary of the critical reservoir properties is provided in Table 1, which includes data on porosity, permeability and other relevant petrophysical and geomechanical parameters.



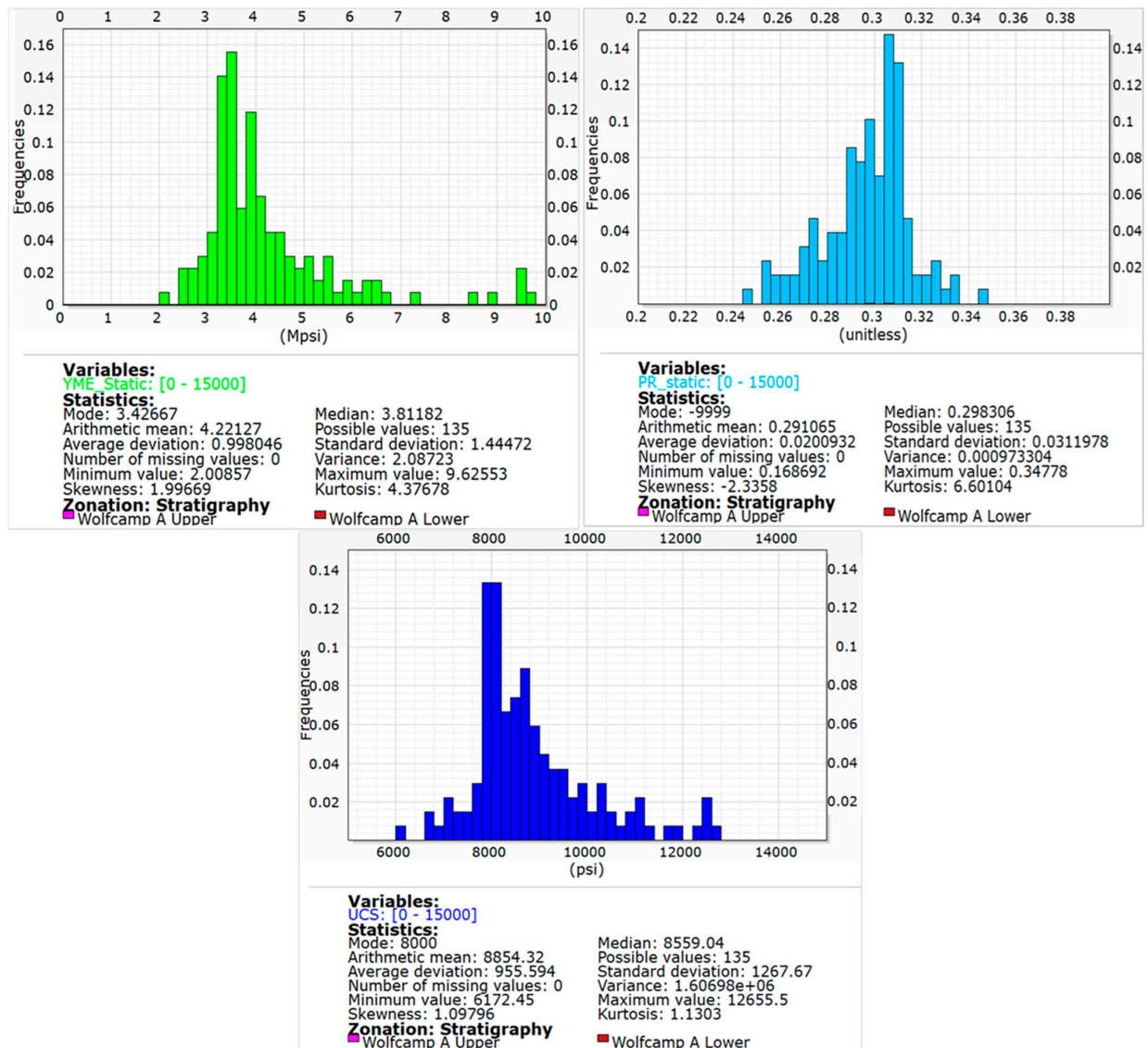


Figure 8. Statistics of rock properties and strength in the Wolfcamp A formation.

Table 1. Summary of reservoir properties.

Properties	Values
Top formation true vertical depth, TVD	11,300 ft
Average reservoir permeability, k	$3.5 \times 10^{-4}$ mD
Average effective matrix porosity, $\phi$	0.04
Reservoir temperature, T	169 F
Initial pore pressure, P	6887 psi
Initial water saturation, Swi	0.6
Critical oil saturation, Soc	0.2
Oil API	43.5
Gas gravity	0.483
Young's modulus of matrix rock, E	$4.22 \times 10^6$ psi
Poisson's ratio of matrix rock, $\nu$	0.297
Overburden stress gradient	1.09 psi/ft
Minimum horizontal stress gradient	0.7 psi/ft
Maximum horizontal stress gradient	0.86 psi/ft

#### 2.4. Simulation of CO<sub>2</sub> Injection

Cyclic CO<sub>2</sub> injection was initiated using the GEM compositional simulator for both wells after five years of primary depleted production. This process aimed to enhance oil recovery by utilizing CO<sub>2</sub> to displace the remaining hydrocarbons in the reservoir, thereby increasing production efficiency and prolonging the production time.

During the injection phase, CO<sub>2</sub> was injected into the reservoir at a constant rate of one million standard cubic feet (MMscf) per day over 30 days. This phase aimed to refill the reservoir's void created by the prior production phase, effectively repressurizing the reservoir above the MMP. The injection was carefully controlled to maintain a BHP limit of 7000 psi to ensure the formation integrity and prevent potential CO<sub>2</sub> leakage. Over the first injection phase, a volume of 30,000 thousand cubic feet (Mcf) of CO<sub>2</sub> was injected into the reservoir. Following the injection phase, a soaking period of 30 days was implemented. During this soaking time, the injected CO<sub>2</sub> was allowed to diffuse and interact with the reservoir fluids, thus swelling the residual oil and decreasing its viscosity. The soaking period is critical as it will enable the CO<sub>2</sub> to effectively mobilize the immobile hydrocarbons. After the soaking period, the reservoir was put back into production for 150 days. This production phase allowed the mobilized hydrocarbons to be produced to the surface, taking advantage of the increased reservoir pressure and improved fluid flow dynamics resulting from the CO<sub>2</sub> injection and soak period.

To verify the efficiency of the CO<sub>2</sub> huff-n-puff process, a total of 28 cycles of CO<sub>2</sub> injection, soaking and production were implemented. Each cycle involved injecting CO<sub>2</sub> at the specified rate, allowing a soak period and producing for the designated time. This repetitive process helped to maximize hydrocarbon recovery and provided valuable data on the performance and effectiveness of cyclic CO<sub>2</sub> injection in enhancing oil recovery.

### 3. Results and Discussion

#### 3.1. Simulation of Fracture Geometry

Well #1 and Well #2 were fractured with 23 and 24 stages, respectively, with the same injection rate, proppant type and amount of fracture fluid. According to fracture reports, the fracture treatment of the two wells is summarized in Table 2. Each stage of the investigated wells is fractured with slick water using 100 mesh and 40/70-mesh sand and 85 barrels per minute (bpm) fluid rate in 103 min.

**Table 2.** Fracture treatment from the field.

	Average Pump Rate per Fracture Stage, bpm	Average Pump Time per Stage, min	Proppant Type
Well #1	85	103	100 mesh; local 40/70 Sand
Well #2	85	103	100 mesh; local 40/70 Sand

When the tensile failure criterion is met, fractures initiate and simultaneously increase the minimum horizontal stress in the adjacent zone, as illustrated in Figure 9. Previous research [4,22,43,45] describes this phenomenon using the concept of stress shadowing. This additional stress due to stress shadowing (represented as red arrows in Figure 9) increases the effective minimum horizontal stress, which, in turn, reduces the likelihood of opening the formation in the desired direction. The direction of fracture propagation may vary depending on the orientation of the existing minimum horizontal stress and the magnitude of the added stress.

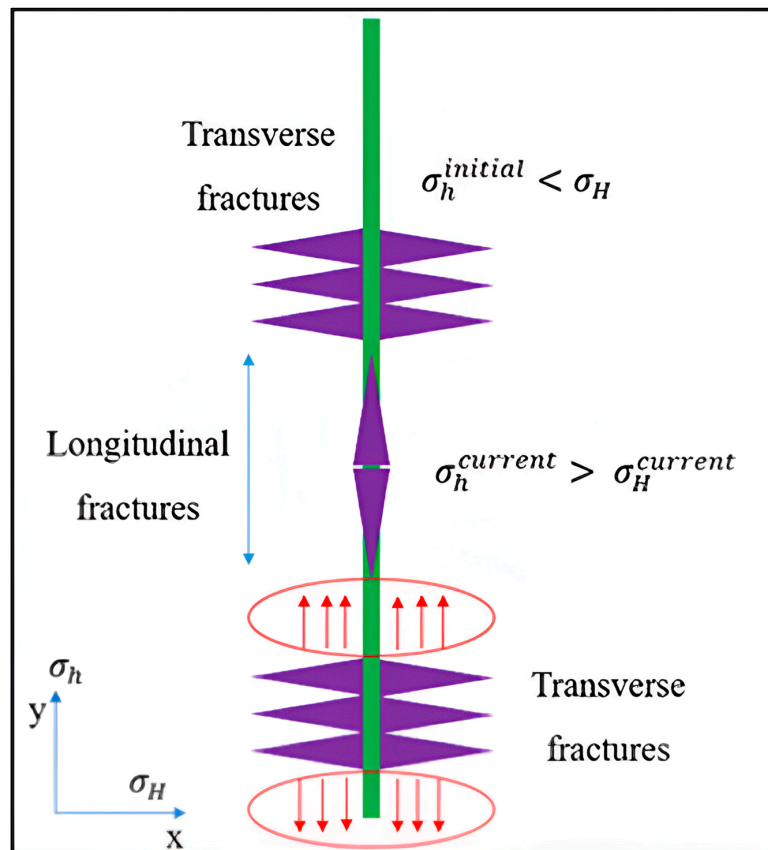


Figure 9. Illustration of stress shadowing effects.

As a result, fractures in such scenarios do not grow symmetrically. Instead, they propagate both transversely and longitudinally, favoring zones of lower effective stress. The fracture simulation results exhibit both symmetric and asymmetric fracture geometries, with fracture lengths ranging from 400 to 1250 feet and fracture heights spanning the entire formation thickness, as shown in Figure 10.

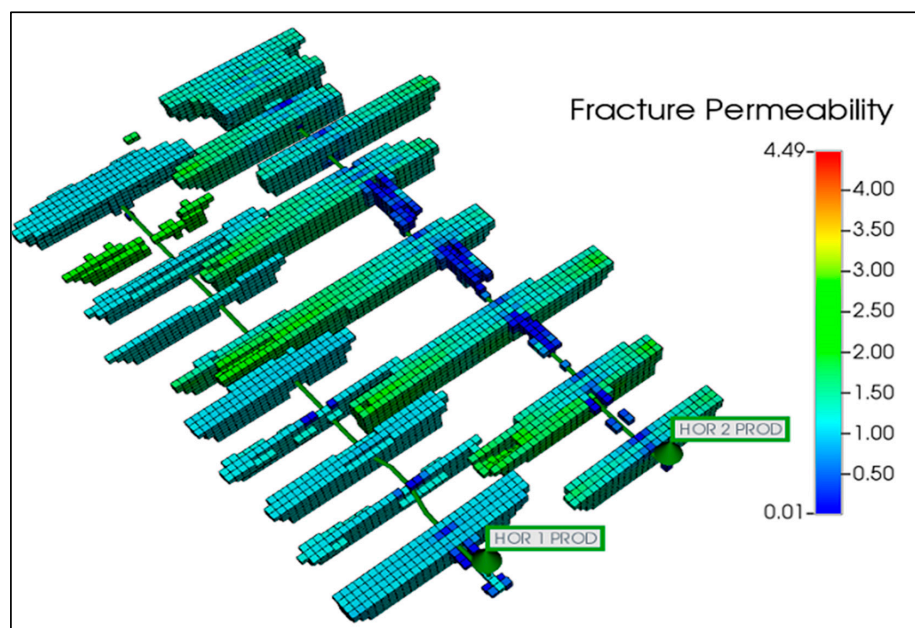


Figure 10. Fracture geometry of Well #1 and Well #2.

### 3.2. Production History Matching

After hydraulic fracturing, Well #1 had been producing for one year before Well #2 was fractured. Several techniques can be deployed to verify the quality of the fracture model. In this study, the production and flowing BHP of the two wells were used as primary references for validation.

For production history matching, various parameters can be adjusted, including reservoir properties, relative permeability curves, fracture and matrix permeability and operational parameters. In unconventional reservoirs, where induced hydraulic fractures are commonly used, post-fractured permeability (or residual fracture permeability) and the relative permeability curves of the fracture system are the most sensitive parameters affecting reservoir fluid flow. To achieve a reasonable matching result, it is crucial to reduce the number of uncertainties considered. Typically, uncertain parameters such as reservoir properties, matrix relative permeability curves and operating conditions are calculated from log data, calibrated using published data or obtained from historical well data. This makes fracture permeability and the relative permeability curves in the fracture system particularly sensitive, as there is limited information available from the literature and laboratory measurements. Consequently, closure fracture permeability, residual fracture permeability and relative permeability curves in the fracture system were treated as the primary varying parameters to achieve production and flowing bottom hole pressure (BHP) matching.

Ojha et al. (2017) [46] measured various shale samples to obtain the average relative permeability curves for the Wolfcamp formation. The relative permeability curves of water–oil and gas–liquid systems from Ojha et al. (2017) [46] were integrated into the base model to simulate multiphase flow. Table 3 lists the parameters considered for matching the production data. Figures 11–13 show the history-matching results for the fluids produced from individual wells. Figure 14 presents the history-matching results for the oil rate and cumulative production of the entire field. The matching results indicate that the quality of the fracture model is sufficient to represent the reservoir accurately for further analyses and forecasting.

**Table 3.** Final history matching parameters.

Matching Parameters	Base Values	Final Values
Closure Fracture Permeability, mD	6	4.8
Residual Fracture Permeability, mD	3	2.4
Fracture Relative Permeability Curves		
Gas relative permeability at connate liquid	0.95	0.9
Oil relative permeability at connate water	0.6	0.7
Oil relative permeability at connate gas	0.6	0.7
Water relative permeability at irreducible oil	0.9	0.85
Curvature exponent of water curve in water–oil system	2	1.5
Curvature exponent of oil curve in water–oil system	2	2
Curvature exponent of gas curve in gas–liquid system	2.4	2.2
Curvature exponent of oil curve in gas–liquid system	2	2
Irreducible water saturation	0.4	0.4
Residual oil saturation in oil–water system	0.2	0.15
Residual (critical) gas saturation	0.05	0.05

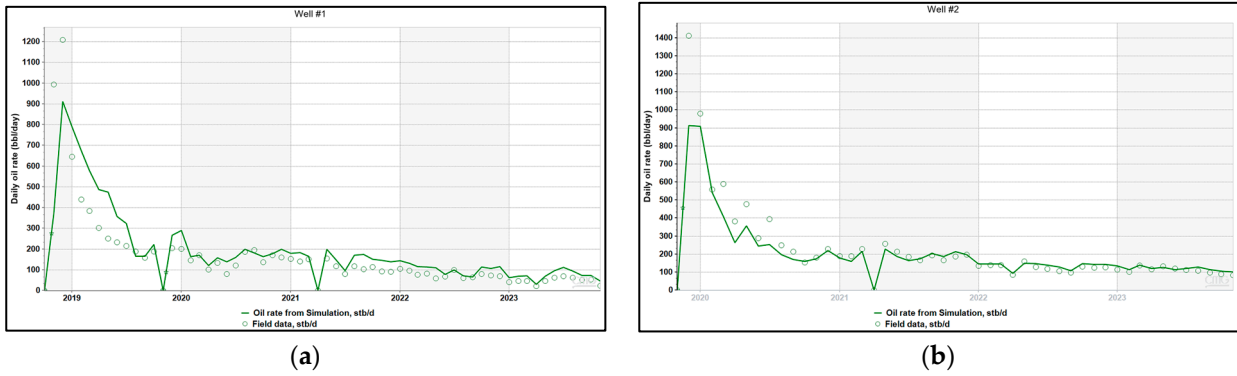


Figure 11. (a) History matching oil rate Well #1; (b) history matching oil rate Well #2.

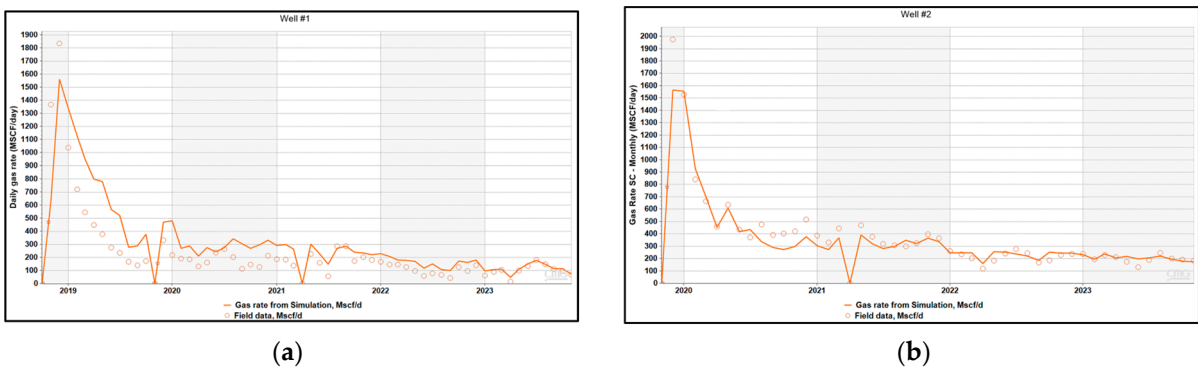


Figure 12. (a) History matching gas rate Well #1; (b) history matching gas rate Well #2.

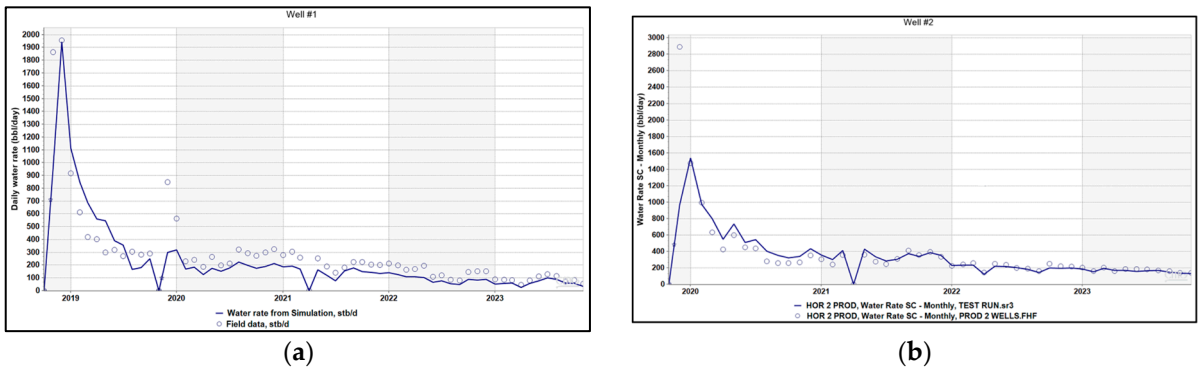


Figure 13. (a) History matching water rate Well #1; (b) history matching water rate Well #2.

### 3.3. Estimating Minimum Miscibility Pressure for CO<sub>2</sub> and the Reservoir's Oil

#### 3.3.1. Oil Composition

The oil composition data (Table 4) and the component properties (Table 5) of PVT for the Wolfcamp A formation are provided below. The composition presented in Table 4 was based on the Bonespring formation laid right above the Wolfcamp A formation [33]. The C7+ fraction has been de-lumped into four pseudo-components to ensure a more accurate PVT model. In this study, PVT calculation and properties interactions among various compositions were performed through an equation-of-state simulator to feed the hydrodynamic modeling performed by numerical simulation. This is the preferred method for the determination of MMP, where the laboratory-measured phase behavior data are available for fine-tuning an equation of state.



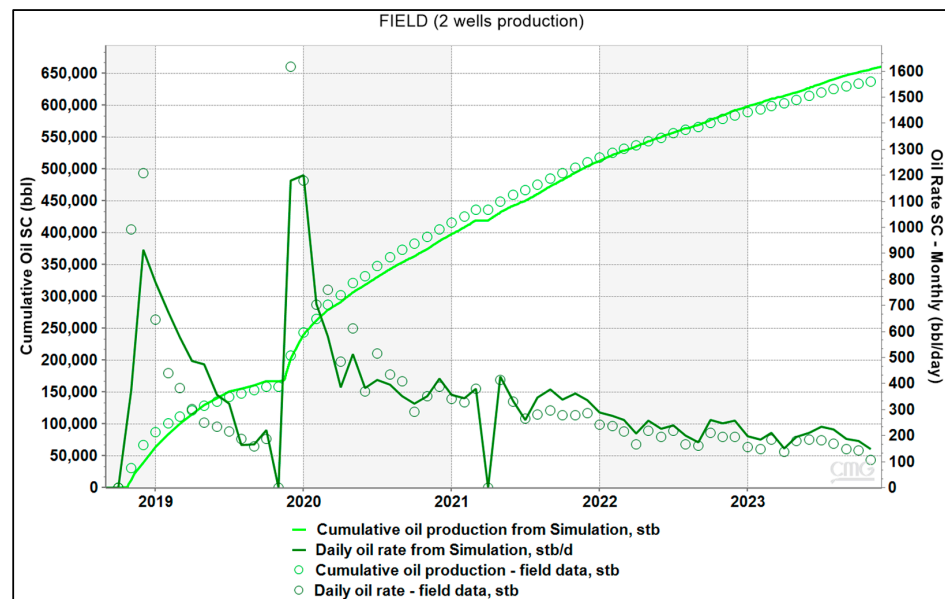


Figure 14. History matching oil cumulative and oil rate of entire field.

Table 4. Fluid composition fraction.

Component	Mole Percent (%)
N <sub>2</sub>	1.07
CO <sub>2</sub>	0.11
CH <sub>4</sub>	46.98
C <sub>2</sub> H <sub>6</sub>	10.66
C <sub>3</sub> H <sub>8</sub>	6.92
IC4	3.22
NC4	1.18
IC5	1.54
NC5	1.21
FC6	1.82
HYP01	7.69
HYP02	10.45
HYP03	5.79
HYP04	1.36

Table 5. Key properties of fluid components.

No.	Component	Pc (atm)	Tc (K)	Acentric Factor	MW	SG
1	N <sub>2</sub>	33.50	126.20	0.04	28.01	0.81
2	CO <sub>2</sub>	72.80	304.20	0.23	44.01	0.82
3	CH <sub>4</sub>	45.40	190.60	0.01	16.04	0.30
4	C <sub>2</sub> H <sub>6</sub>	48.20	305.40	0.10	30.07	0.36
5	C <sub>3</sub> H <sub>8</sub>	41.90	369.80	0.15	44.10	0.51
6	IC4	36.00	408.10	0.18	58.12	0.56
7	NC4	37.50	425.20	0.19	58.12	0.58
8	IC5	33.40	460.40	0.23	72.15	0.63
9	NC5	33.30	469.60	0.25	72.15	0.63
10	FC6	32.46	507.50	0.28	86.00	0.69
11	HYP01	30.79	570.66	0.28	102.13	0.76
12	HYP02	21.84	670.57	0.46	157.05	0.81
13	HYP03	14.12	802.17	0.76	264.75	0.87
14	HYP04	9.45	943.83	1.14	452.25	0.93

### 3.3.2. MMP Determination

In CO<sub>2</sub>-EOR design, the MMP is a crucial parameter for improving oil recovery from the porous medium and achieving maximum displacement efficiency. MMP is defined as the lowest pressure at which the injected gas becomes dynamically miscible with the reservoir oil. Although MMP can be accurately measured using laboratory experimental methods, these methods are often costly and time-consuming [36]. Therefore, in this research, the slim tube test was simulated using a one-dimensional compositional reservoir model.

To estimate the MMP between the injected CO<sub>2</sub> and the oil composition for the study area—the Wolfcamp A reservoir—a comprehensive suite of slim tube simulations was conducted using the CMG-GEM software 2024.20.5.811. These simulations are essential for determining the pressure at which CO<sub>2</sub> can effectively mix with the reservoir oil without forming two separate phases. By conducting these slim tube simulations, which mimic the reservoir conditions and fluid interactions, it was able to accurately establish an MMP of approximately 4300 psi (Figure 15). This value is critical for designing and optimizing enhanced oil recovery processes, as it ensures that the injected CO<sub>2</sub> will efficiently mix with the reservoir oil, thereby improving recovery rates and maximizing production from the investigated formation.

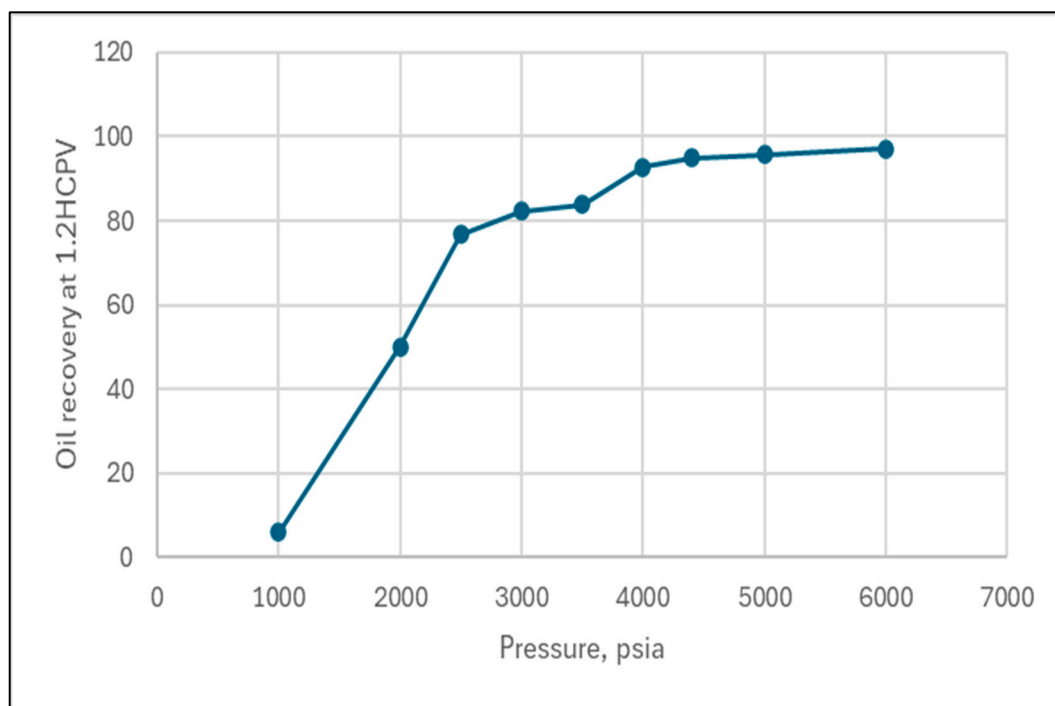


**Figure 15.** Slim-tube simulation result for MMP.

Also, a cell-to-cell simulation was conducted using the aforementioned PVT fluid model with pure CO<sub>2</sub> injection to compare with 1D slim-tube simulation and to better understand the miscibility behavior between the CO<sub>2</sub> and reservoir oil. This simulation was performed using the CMG-Winprop simulator, allowing for a detailed examination of how CO<sub>2</sub> interacts with the oil at different pressures and temperatures. The results from this simulation indicated that the MMP is approximately 4125 psi (Figure 16). It represents the phase diagram of the fluid. The blue and red lines indicate the phase transition from liquid to a two-phase liquid-gas state and then to a fully gas phase. Accurately estimating the MMP for the Wolfcamp A shale formation is crucial for optimizing CO<sub>2</sub> injection strategies and ensuring the successful implementation of the CO<sub>2</sub> huff-n-puff technique in unconventional formations.

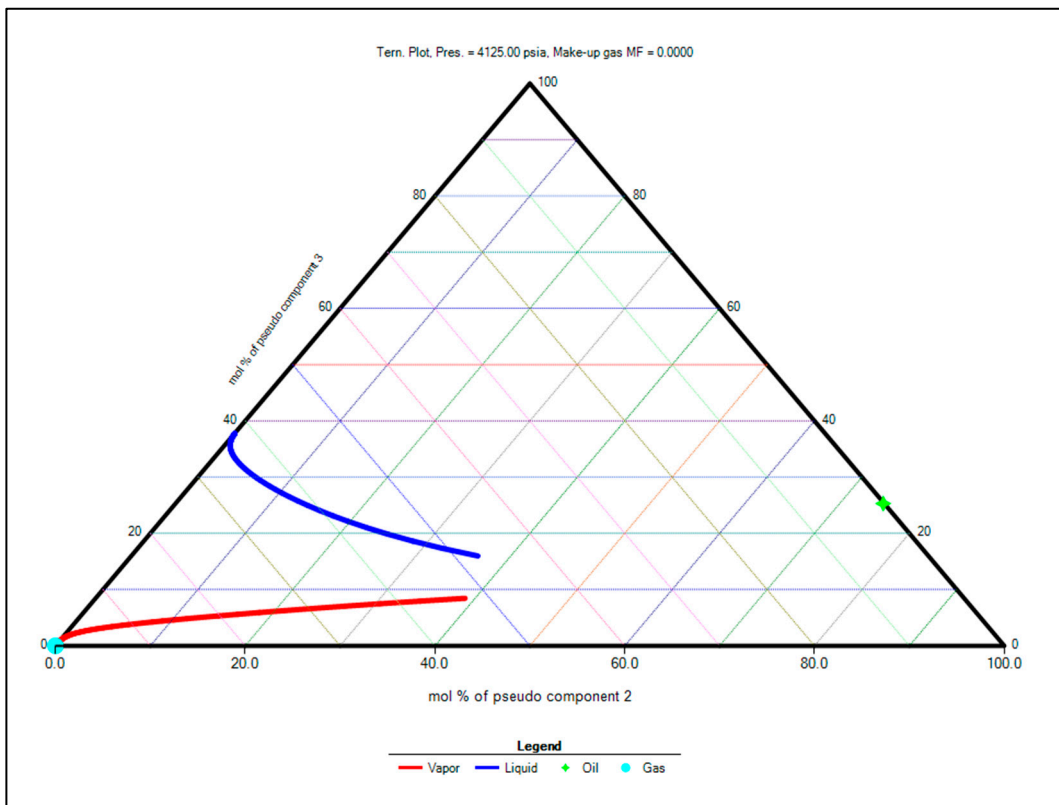


Figure 16. Cell-to-cell simulation result for MMP.

### 3.4. Modeling of Cyclic CO<sub>2</sub> Injection

The modeling of the CO<sub>2</sub> huff-n-puff application involves 28 consecutive cycles, covering a production period of 10 years. These cycles include a repetitive process of cyclic CO<sub>2</sub> injection, soaking and production. The results are shown in Figure 17. (a) Cumulative oil production of Well #1 associated with 1 MMscf/d CO<sub>2</sub> injection and (b) cumulative oil production of Well #2 associated with 1 MMscf/d CO<sub>2</sub> injection are for both studied wells, with the CO<sub>2</sub> being injected at a consistent rate of 1 million standard cubic feet per day per well (MMscf/d/well).

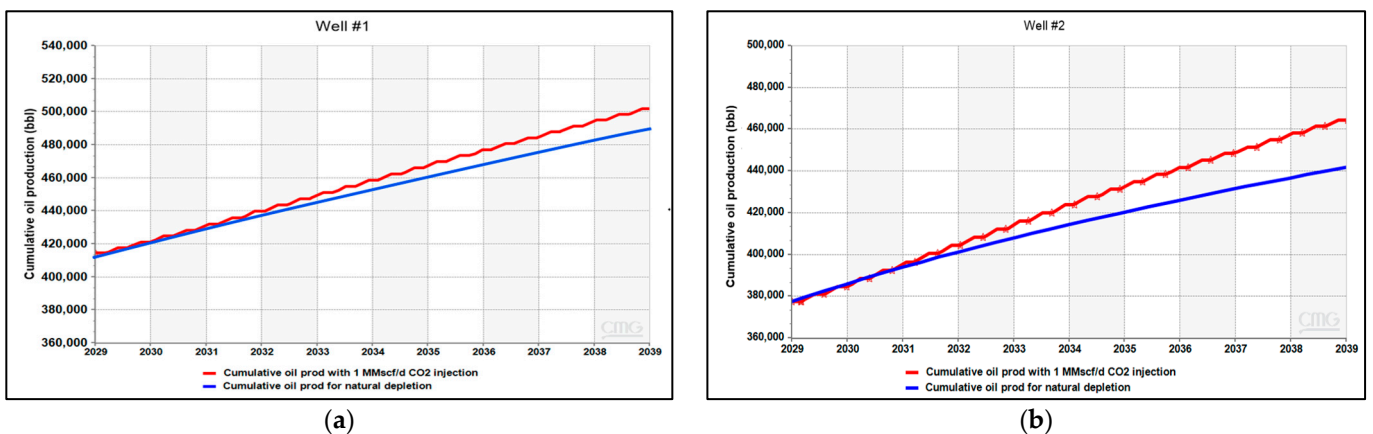


Figure 17. (a) Cumulative oil production of Well #1 associated with 1 MMscf/d CO<sub>2</sub> injection; (b) cumulative oil production of Well #2 associated with 1 MMscf/d CO<sub>2</sub> injection.

Figure 17 compares cumulative oil production between the enhanced case and the base case, in which no CO<sub>2</sub> injection was deployed for both wells. Well #1 shows an improvement of 2% in cumulative oil, whereas Well #2 expresses a development of 6%

using the CO<sub>2</sub> huff-n-puff technique. Specifically, the incremental oil production from Well #2 is approximately 28,000 STB, representing a 6.3% improvement over primary depletion. In contrast, Well #1 exhibits a significantly lower increment of 10,000 STB, corresponding to only a 2% production enhancement. The difference in CO<sub>2</sub>-EOR percentage between the two wells comes from production starting time and treatment additives in the fracturing fluid. Note that Well #1 started producing one year before the fracturing of Well #2, so the absolute cumulative oil production without CO<sub>2</sub> enhancement was higher than that of Well #2, making the percentage of oil increment in Well #1 lower than that of Well #2. On the other hand, although both wells were hydraulically fractured by slick water, the additive’s concentration differed. Well #2 was treated with a higher concentration of hydrochloric acid, salts and corrosion inhibitors than Well #1, indicating an improved downhole treatment, which can further aid in the tertiary recovery process using CO<sub>2</sub> injection.

With the difference in downhole treatment between the two wells, the marked disparity in production improvement is hypothesized to be primarily attributable to formation damage in Well #1. However, analyzing formation damage mechanisms on the production performance of Well #1 is out of the scope of this study and will be scrutinized in future work. Given this substantial performance differential between the two wells, subsequent sensitivity analyses will focus exclusively on Well #2 to optimize production parameters and better understand the factors influencing EOR in this reservoir.

### 3.5. Cyclic Times Sensitivity

For each scenario, a total of 24 cycles of CO<sub>2</sub> huff-n-puff were simulated on Well #2. The total time of one cycle is 150 days, with injection, soak and production periods varying to determine the optimal operating conditions. The cumulative volume of CO<sub>2</sub> injection each cycle was 30 MMscf. A summary of various CO<sub>2</sub> huff-n-puff strategies is presented in Table 6. The ultimate goal of this sensitivity analysis is to maximize total oil recovery. Table 7 summarizes the simulation parameters and results. Compared to the base case with no CO<sub>2</sub> injection, the oil recovery improved by 4% to 8%.

**Table 6.** Summary of different CO<sub>2</sub> huff-n-puff strategy.

Case Number	CO <sub>2</sub> Injection Rate, MMscf/d	Injection Time, Day	Soaking Time, Day	Production Time, Day
Case 1	1	30	30	90
Case 2	1	30	20	100
Case 3	1	30	50	70
Case 4	1	30	10	110
Case 5	0.5	60	15	75
Case 6	2	15	20	115
Case 7	2	15	10	125
Case 8	2	15	30	105

**Table 7.** Summary of CO<sub>2</sub>-EOR process.

Scenario	Cumulative Oil Production		Cumulative CO <sub>2</sub>		Estimated CO <sub>2</sub> Storage (mil.lbs)
	Total (STB)	Incremental EOR (STB)	Injection (mil.lbs)	Production (mil.lbs)	
Base case (no CO <sub>2</sub> -EOR)	441,912	Not applicable			
Case 1	469,891	27,979	87.51	66.52	20.99
Case 2	467,252	25,340	87.51	71.87	15.64
Case 3	464,271	22,359	87.51	69.81	17.7
Case 4	469,820	27,908	87.51	74.68	12.84
Case 5	459,431	17,519	87.01	76.55	10.45
Case 6	472,894	30,982	87.51	74.01	13.51
Case 7	472,773	30,861	87.51	69.56	17.95
Case 8	464,480	22,568	87.51	68.04	19.47

Although the eight scenarios presented in Table 7 utilize the same amount of CO<sub>2</sub> injection of 87.51 million pounds (mil.lbs), Case 1 shows the highest CO<sub>2</sub> storage capacity of 20.99 mil.lbs, while Case 6 and Case 7 provide the highest oil recovery of 472,894 stock tank barrels (STBs) and 472,773 STBs, respectively. Considering CO<sub>2</sub> storage, Case 1, with the cyclic time shown in Table 7, clearly sequesters approximately 55% more CO<sub>2</sub> than Case 6 and about 17% more than Case 7. Thus, Case 1 stands out as the most effective strategy in terms of CO<sub>2</sub> sequestration. However, this advantage comes with a trade-off in oil production since Case 1 yields approximately 9.7% less oil than Case 6 and 9.3% less than Case 7. Considering CO<sub>2</sub> storage and oil recovery efficiency simultaneously, Case 1 provides the most balanced performance. Additionally, Case 8 shows the second highest CO<sub>2</sub> storage at 19.47 mil.lbs, but its oil production is much lower than that of Cases 1, 6 and 7. Therefore, Case 1 remains the best option to address both CO<sub>2</sub> storage capacity and hydrocarbon recovery.

Diving into different cyclic strategies, it is worth mentioning that, although the total amount of injected CO<sub>2</sub> is the same for every case, Case 1 implements a lower injection rate of 1 million cubic feet per day (MMscf/d) over 30 days, while Case 6 and Case 7 utilize a higher injection rate of 2 MMscf/d over a shorter period of 15 days. Furthermore, Case 5, which has the lowest injection rate of 0.5 MMscf/d spanning over 60 days of injection, showed the least efficiency of CO<sub>2</sub> storage and oil recovery. The discrepancies in oil recovery and CO<sub>2</sub> storage indicate that the variation in injection time and rate are decisive factors in the CO<sub>2</sub> huff-n-puff process.

### 3.6. CO<sub>2</sub> Volume Injection Sensitivity

The cyclic time sensitivity analysis was derived from Case 1, with the injection rate varying from 1 MMscf to 25 MMscf per day, and the maximum bottom hole injection pressure was set at 7000 psi or 80% of fracture pressure to avoid any risk of formation integrity. Table 8 presents the oil production increments associated with various CO<sub>2</sub> injection rates. Based on the simulation results, the cumulative oil production and estimated CO<sub>2</sub> storage increase proportionally with the CO<sub>2</sub> injection rate when the injection rate varies from 1 MMscf/d to 20 MMscf/d. The cumulative oil recovery in this range rises from 6.3% to 68.8% due to the EOR process. This linear relationship indicates that better performance in enhancing oil recovery can be achieved by maximizing the CO<sub>2</sub> injection rate within the surface equipment's capacity. In addition, maximizing the injection rate aids in maintaining reservoir pressure at or above the MMP at 4300 psi, which is the most critical factor in extracting residual oil in the CO<sub>2</sub>-EOR process. On the other hand, since more CO<sub>2</sub> can dissolve into formation brine at higher pressure, according to Henry's law (1803), maintaining a high injection rate increases CO<sub>2</sub> solubility, thereby enhancing CO<sub>2</sub> dispersion throughout the hydraulic fracture network and rock matrix. This combined effect contributes to boosting oil recovery and also improving sequestration significantly.

**Table 8.** Effect of various CO<sub>2</sub> injection rates on enhanced oil recovery.

Scenario	Cumulative Oil Production		Cumulative CO <sub>2</sub>		Estimated CO <sub>2</sub> Storage (mil.lbs)
	Total (STB)	Incremental EOR (STB)	Injection (mil.lbs)	Production (mil.lbs)	
Primary depletion	441,912	Not applicable			
1 MMscf/d	469,891	27,979	87.51	66.52	20.99
7 MMscf/d	577,219	135,307	875.12	778	97.12
10 MMscf/d	605,789	163,877	1050.14	926.78	123.37
15 MMscf/d	643,661	201,749	1312.68	1143.17	169.51
20 MMscf/d	745,900	303,988	1742.00	1566.18	175.82
25 MMscf/d	748,371	306,459	1931.41	1733.94	197.47



However, increasing the CO<sub>2</sub> injection rate further, from 20 MMscf/d to 25 MMscf/d, only boosts the increment by 0.5%. Therefore, the optimal injection rate was determined at 20 MMscf/d. At this rate, oil production reaches its highest incremental rate due to the CO<sub>2</sub> huff-n-puff process, which also gives the highest CO<sub>2</sub> storage efficiency. Moving above a 20 MMscf/d injection rate increases operational costs and CO<sub>2</sub> requirements without a proportional increase in oil production and estimated CO<sub>2</sub> storage. This finding is also demonstrated in Figure 18, which shows that the cumulative oil increasing rate slows down significantly at the injection rate higher than 20 MMscf/d.

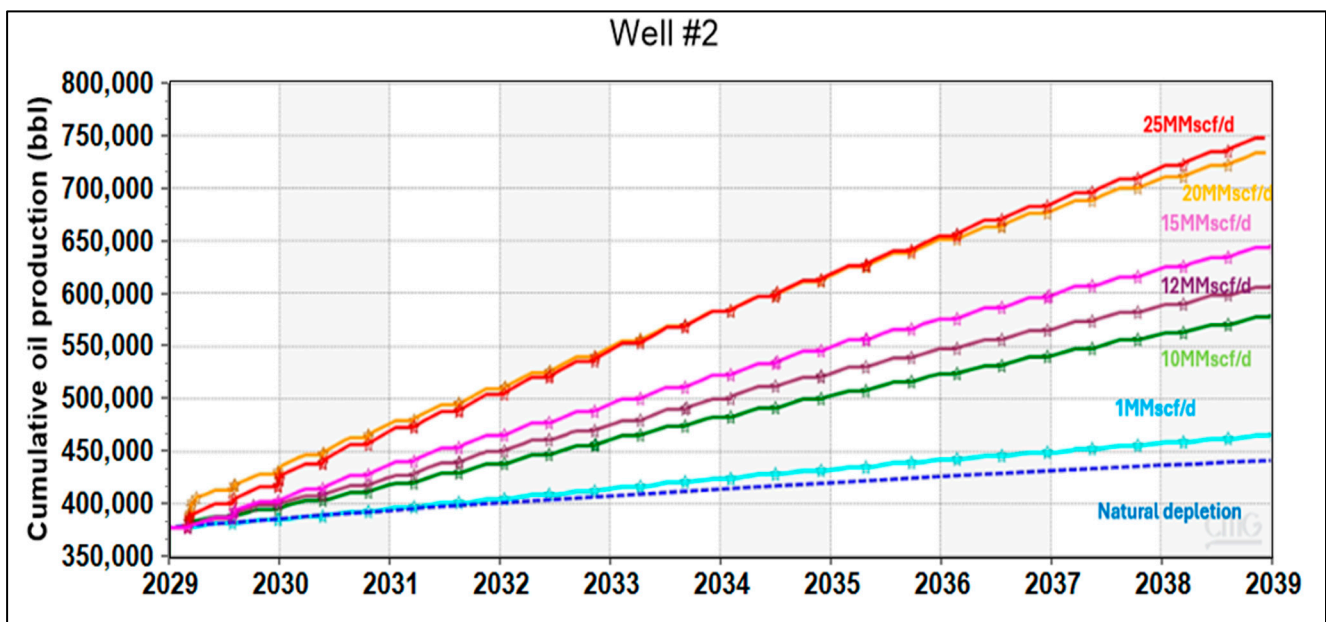


Figure 18. Cumulative oil production corresponding with different CO<sub>2</sub> injection rates.

Figure 19 expresses the mass of CO<sub>2</sub> storage corresponding with different CO<sub>2</sub> injection rates. When the injection rate increases from 1 MMscf/d to 20 MMscf/d, the total amount of CO<sub>2</sub> storage increases significantly from 10,000 to 80,000 tonnes over ten years. From 20 to 25 MMscf/d, the CO<sub>2</sub> storage only increased by 10,000 tonnes. This observation emphasizes the importance of performing sensitivity analysis on the CO<sub>2</sub> injection rate because it supports operators in determining the suitable rate considering the supplement of CO<sub>2</sub>. It is worth mentioning that CO<sub>2</sub> supply is one of the most expensive and decisive components relating to field development and management. Additionally, the more CO<sub>2</sub> is injected, the higher the required capacity of surface equipment. Finally, the CO<sub>2</sub> injection rate should comply with the maximum allowable injection pressure allowed by law to avoid any unintentionally induced fractures in the formation. By adopting these results, one can optimize CO<sub>2</sub> huff-n-puff operational costs while maximizing oil recovery.

Figure 20 compares the CO<sub>2</sub> mole fraction within the hydraulic fracture network under two different gas injection scenarios: 1 MMscf/d and 20 MMscf/d. The data clearly show that, with the higher injection rate of 20 MMscf/d, CO<sub>2</sub> penetrates deeper and spreads more extensively throughout the fracture network and rock matrix. This deeper penetration facilitates better mixing with the residual oil in the reservoir. Consequently, it achieves more oil swelling in the 20 MMscf/d scenario, hence improving the recovery factor considerably. Figures 21 and 22 illustrate the pressure distribution and reservoir pressure histogram after ten years of CO<sub>2</sub> injection for 1 MMscf/d and 20 MMscf/d scenarios, respectively. As depicted in Figure 21, at the conclusion of the injection period, the majority of the reservoir pressure remains below the MMP. This insufficient pressure results in lower oil recovery because CO<sub>2</sub> does not mix well with the residual oil, failing to form a single miscible phase. In other words, at 1 MMscf/d, the CO<sub>2</sub> remains largely immiscible, making the huff-n-puff

process less effective. In contrast, Figure 22 demonstrates that, with a 20 MMscf/d injection rate, most of the fracture network in Well #2 is at a pressure above the MMP after ten years of CO<sub>2</sub> injection. By maintaining reservoir pressure at a high level, it ensures the solubility of CO<sub>2</sub> in the residual oil, yielding substantial oil recovery and a significant amount of CO<sub>2</sub> sequestration.

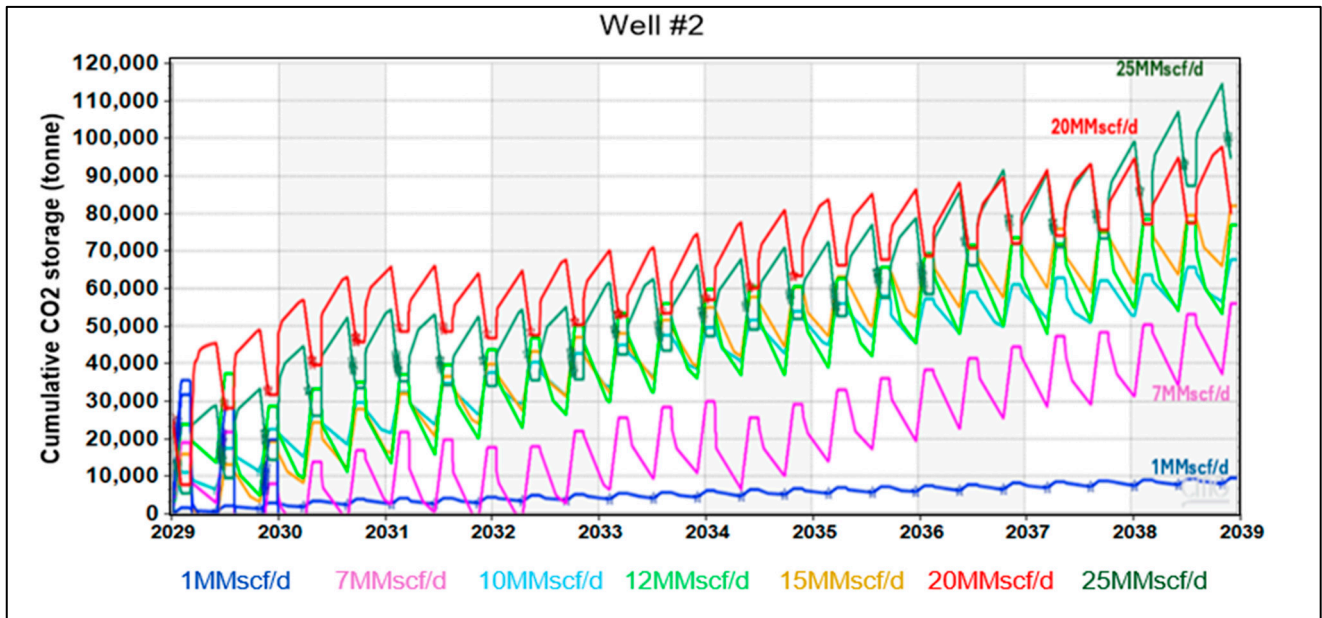


Figure 19. CO<sub>2</sub> storage mass corresponding with various CO<sub>2</sub> injection rates.

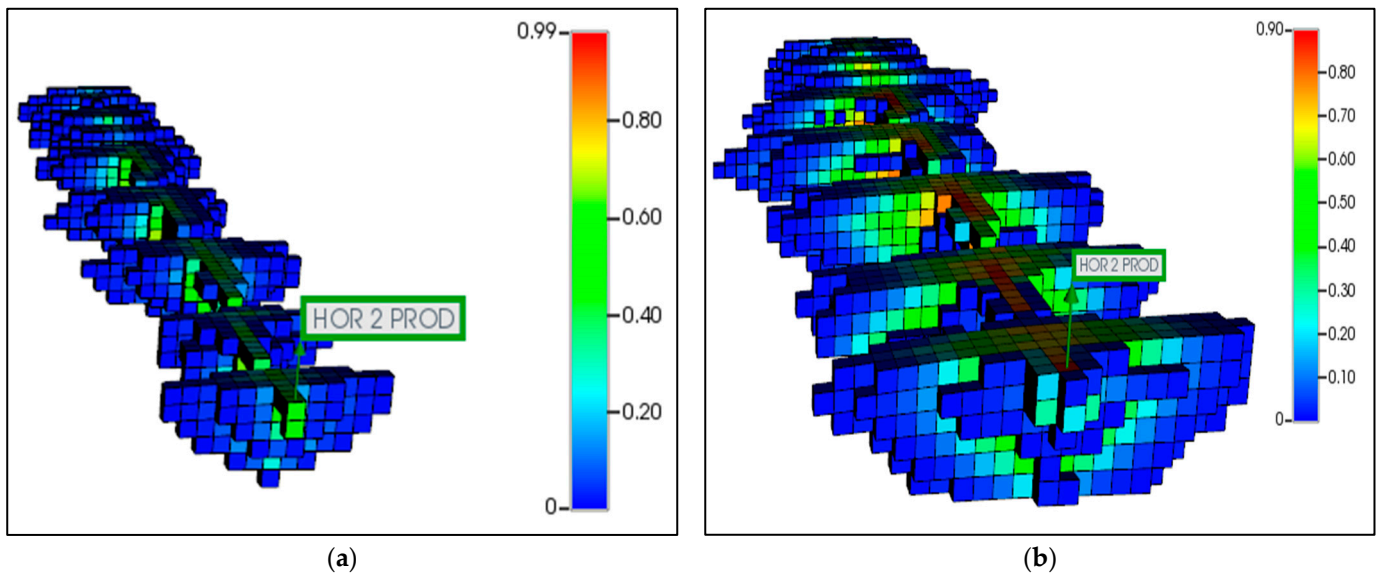


Figure 20. (a) CO<sub>2</sub> mole fraction in fracture network with 1 MMscf/d injection rate; (b) CO<sub>2</sub> mole fraction in fracture network with 20 MMscf/d injection rate.

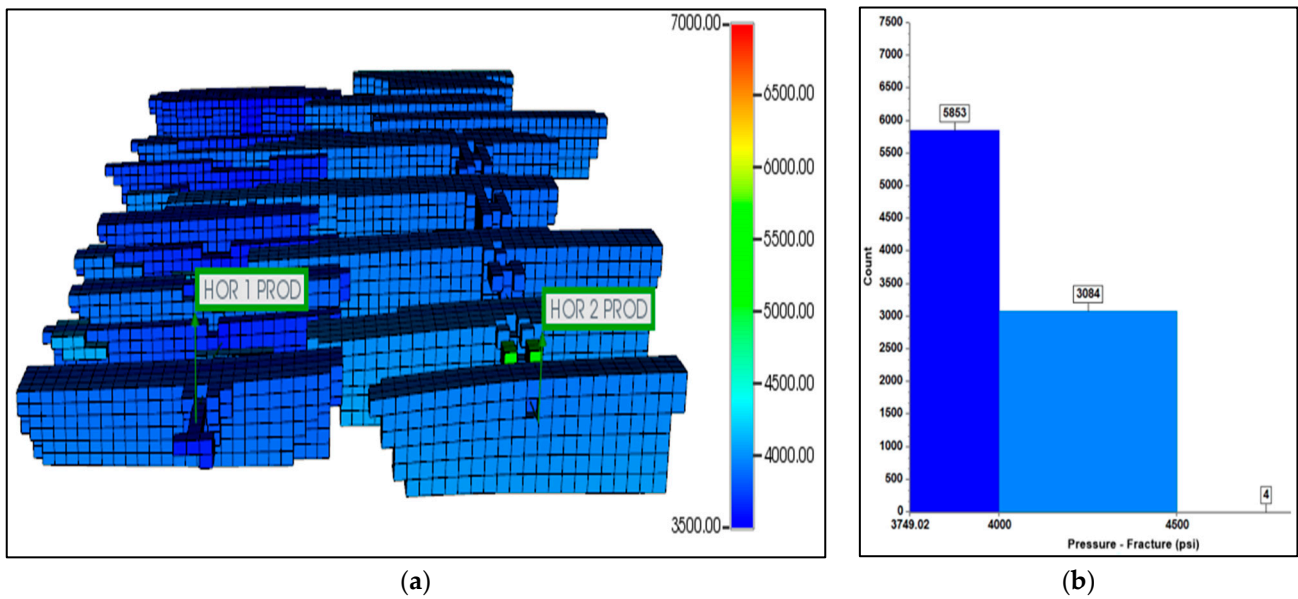


Figure 21. (a) Pressure distribution after 10 years with 1 MMscf/d of CO<sub>2</sub> injection; (b) pressure histogram at the end of CO<sub>2</sub> huff-n-puff simulation.

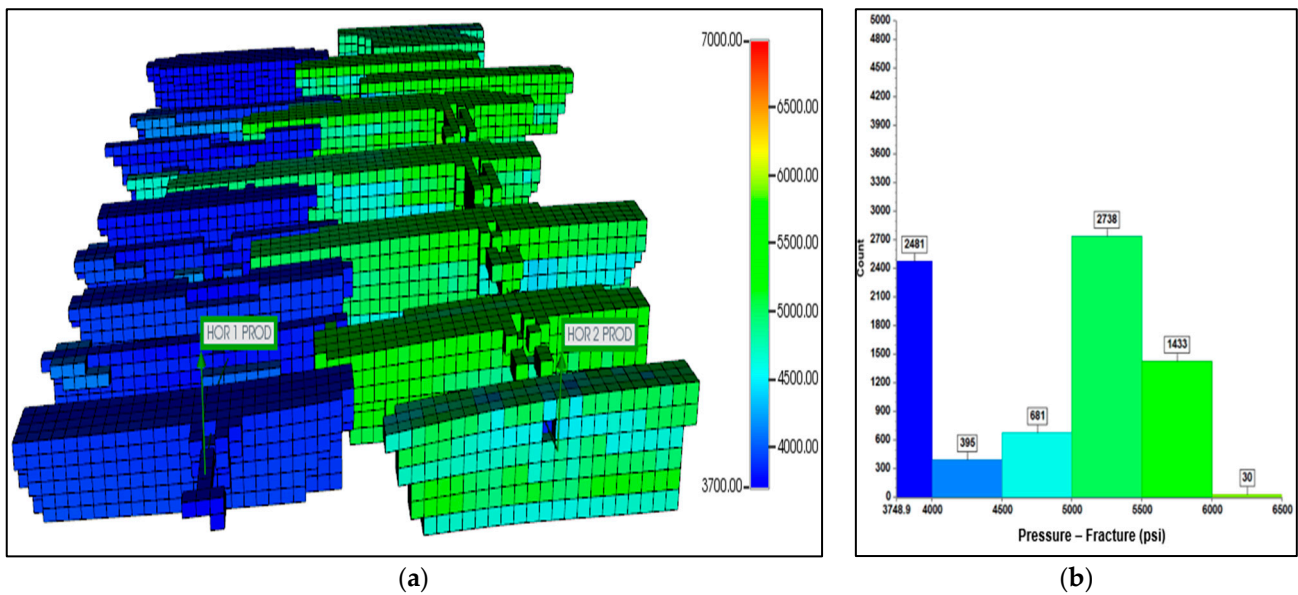


Figure 22. (a) Pressure distribution after 10 years with 20 MMscf/d of CO<sub>2</sub> injection; (b) pressure histogram at the end of CO<sub>2</sub> huff-n-puff simulation.

Summarizing the above analyses, a procedure aimed at optimizing CO<sub>2</sub> huff-n-puff for depleted hydraulically fractured wells can be outlined as follows:

- Determine the maximum allowable injection pressure and injection rate without causing the potential risk of breaking the formation.
- Start injecting the maximum allowable rate and monitor reservoir pressure at or above MMP.
- Keep operating with the highest determined rate to achieve the dual objectives of maximizing oil recovery and CO<sub>2</sub> storage.
- If the CO<sub>2</sub> supply shortage happens, gradually reduce the current injection rate while closely monitoring EOR and sequestration performance. Rerun the volume injection sensitivity if necessary to assist in decision-making.

Last but not least, this study generated a synthetic database through various full simulation runs, which can be used to apply machine learning techniques to optimize CO<sub>2</sub> huff-n-puff operations further. Machine learning can aid in generating proxy models, which serve as mathematical representations of fully physics reservoir simulations. Through proxy models, the computational costs associated with running complex coupled geomechanical–hydrodynamic models will be reduced significantly [47]. Several machine learning algorithms can be implemented to facilitate the optimization process and support decision-making for more extensive field development. Future work will aim to incorporate machine learning into the optimization process.

#### 4. Conclusions

This study presents a novel and systematic approach exploiting numerical simulation to optimize the CO<sub>2</sub> huff-n-huff process for enhancing oil recovery in depleted hydraulic fracture wells, specifically within the Wolfcamp A formation of the Delaware Basin. Through sensitivity analysis of CO<sub>2</sub> injection rates and cycle times, this research determined an optimal cycle time with 30 days of injection, 30 days of soaking and 90 days of production. This finding implies that a ratio of 1:1:3 for injection, soaking and producing is optimal for the research formation. The ideal scenario of the pilot well, using a gas injection rate of 20 MMscf/d, demonstrated a remarkable 68.8% improvement in cumulative oil recovery compared to natural depletion while efficiently sequestering approximately 80,000 tonnes of CO<sub>2</sub> in the depleted hydraulic fractured network over ten years.

The key novelties of this research lie in the comprehensive workflow, which integrates coupled models with practical field data to develop an accurate representation of the field and perform optimization of oil recovery and CO<sub>2</sub> sequestration. All uncertainties from reservoir properties and the hydraulic fracturing process are taken into consideration. The proposed approach is not only applicable to the Wolfcamp A formation but can also be adopted by industry for other unconventional reservoirs in the U.S. As the number of depleted hydraulic fracture wells keeps increasing rapidly in the future, findings from this research provide valuable and handy guidance for deploying CO<sub>2</sub> huff-n-puff in those potential candidates to achieve both economic and environmental purposes.

**Author Contributions:** Conceptualization, D.B.; methodology, D.B., D.P., S.N. and K.N.; software, D.B., D.P. and K.N.; validation, D.B., D.P. and K.N.; formal analysis, S.N. and K.N.; investigation, D.B., D.P. and K.N.; resources, D.B. and D.P.; data curation, D.B., D.P., S.N. and K.N.; writing—original draft preparation, D.B., D.P., S.N. and K.N.; writing—review and editing, D.B., D.P., S.N. and K.N.; visualization, D.B.; supervision, D.B.; project administration, D.B. and D.P.; funding acquisition, D.B. All authors have read and agreed to the published version of the manuscript.

**Funding:** This research received no external funding.

**Data Availability Statement:** The original contributions presented in this study are included in the article, further inquiries can be directed to the corresponding author.

**Acknowledgments:** The authors wish to thank the New Mexico Institute of Mining and Technology and Petroleum Recovery Research Center for supporting the authors in accomplishing this work.

**Conflicts of Interest:** The authors declare no conflicts of interest.

#### References

1. Energy Information Administration. *Annual Energy Outlook 2023*; EIA: Washington, DC, USA, 2023.
2. Wachtmeister, H.; Lund, L.; Aleklett, K.; Hook, M. Production Decline Curves of Tight Oil Wells in Eagle Ford Shale. *Nat. Resour. Res.* **2017**, *26*, 365–377. [[CrossRef](#)]
3. Shabib-Asl, A.; Chen, S.; Zheng, S. Performance of CO<sub>2</sub> Foam Huff and Puff in Tight Oil Reservoirs. *Front. Energy Res.* **2022**, *10*, 826469. [[CrossRef](#)]
4. Ding, D.Y.; Langouet, H.; Jeannin, L. Simulation of fracturing-induced formation damage and gas production from fractured wells in tight gas reservoirs. *SPE Prod. Oper.* **2013**, *28*, 246–258. [[CrossRef](#)]
5. Guo, B.; Gao, D.; Qianjun, W. The Role of Formation Damage in Hydraulic Fracturing Shale Gas Wells. In Proceedings of the SPE Eastern Regional Meeting, Columbus, OH, USA, 17–19 August 2011.



6. Bottero, S.; Picioreanu, C.; Enzien, M.; van Loosdrecht, M.C.; Bruining, H.; Heimovaara, T. Formation Damage and Impact on Gas Flow Caused by Biofilms Growing Within Proppant Packing Used in Hydraulic Fracturing. In Proceedings of the SPE International Symposium and Exhibition on Formation Damage Control, Lafayette, LA, USA, 10–12 February 2010.
7. Khurshid, I.; Al-Shalabi, E.W.; Al-Attar, H.; Ahmed, K.A. Characterization of Formation Damage and Fracture Choking in Hydraulically Induced Fractured Reservoirs Due to Asphaltene Deposition. In Proceedings of the SPE Gas & Oil Technology Showcase and Conference, Dubai, United Arab Emirates, 21–23 October 2019.
8. Male, F.; Duncan, I.J. The paradox of increasing initial oil production but faster decline rates in fracking the Bakken Shale: Implications for long term productivity of tight oil plays. *J. Pet. Sci. Eng.* **2022**, *208*, 109406. [[CrossRef](#)]
9. Zhou, X.; Yuan, Q.; Peng, X.; Zeng, F. A critical review of the CO<sub>2</sub> huff ‘n’ puff process for enhanced heavy oil recovery. *Fuel* **2018**, *215*, 813–824. [[CrossRef](#)]
10. Liu, J.; Li, H.; Tan, Q.; Liu, S.; Zhao, H.; Wang, Z. Quantitative study of CO<sub>2</sub> huff-n-puff enhanced oil recovery in tight formation using online NMR technology. *J. Pet. Sci. Eng.* **2022**, *216*, 110688. [[CrossRef](#)]
11. Rojas, G.A.; Ali, S.M. Dynamics of Subcritical CO<sub>2</sub>/Brine Floods for Heavy-Oil Recovery. *SPE Reserv. Eng.* **1988**, *3*, 35–44. [[CrossRef](#)]
12. Jeong, M.S.; Lee, K.S. Maximizing oil recovery for CO<sub>2</sub> huff and puff process in pilot scale reservoir. In Proceedings of the World Congress on ACEM15, Icheon, Republic of Korea, 25–29 August 2015.
13. Holm, L.W.; Josendal, V.A. Effect of Oil Composition on Miscible-Type Displacement by Carbon Dioxide. *SPE J.* **1982**, *22*, 87–98. [[CrossRef](#)]
14. Nguyen, P.; Carey, Viswanathan, H.S.B.; Porter, M. Effectiveness of supercritical-CO<sub>2</sub> and N<sub>2</sub> huff-and-puff methods of enhanced oil recovery in shale fracture networks using microfluidic experiments. *Appl. Energy* **2018**, *230*, 160–174. [[CrossRef](#)]
15. Wawrzyńczak, D.; Panowski, M.; Majchrzak-Kuceba, I. Possibilities of CO<sub>2</sub> purification coming from oxy-combustion for enhanced oil recovery and storage purposes by adsorption method on activated carbon. *Energy* **2019**, *180*, 787–796. [[CrossRef](#)]
16. Seyyedsar, S.M.; Farzaneh, S.; Sohrabi, M. Investigation of low-density CO<sub>2</sub> injection for enhanced oil. *Ind. Eng. Chem. Res.* **2017**, *56*, 5443–5454. [[CrossRef](#)]
17. Bank, G.; Riestenberg, D.; Koperna, G. CO<sub>2</sub>-Enhanced Oil Recovery Potential of the Appalachian Basin. In Proceedings of the Eastern Regional Meeting, Lexington, KY, USA, 17–19 October 2007.
18. Yu, W.; Lashgari, H.; Sephehrnoori, K. Simulation Study of CO<sub>2</sub> Huff-n-Puff Process in Bakken Tight Oil Reservoirs. In Proceedings of the Society of Petroleum Engineers Western North America and Rocky Mountain Joint Conference and Exhibition, Denver, CO, USA, 15–18 April 2014.
19. Ning, Y.; Tura, A. Economic and operational investigation of CO<sub>2</sub> sequestration through enhanced oil recovery in unconventional reservoirs in Colorado, USA. *Geoenery Sci. Eng.* **2023**, *226*, 211820. [[CrossRef](#)]
20. Zhao, J.; Wang, P.; Yang, H.; Tang, F.; Ju, Y.; Jia, Y. Experimental Investigation of the CO<sub>2</sub> Huff and Puff Effect in Low-Permeability Sandstones with NMR. *ACS Omega* **2021**, *6*, 15601–15607. [[CrossRef](#)]
21. Afari, S.; Ling, K.; Sennaoui, B.; Maxey, D.; Oguntade, T.; Porlles, J. Optimization of CO<sub>2</sub> huff-n-puff EOR in the Bakken Formation using numerical simulation and response surface methodology. *J. Pet. Sci. Eng.* **2022**, *215*, 110552. [[CrossRef](#)]
22. Song, C.; Yang, D. Experimental and numerical evaluation of CO<sub>2</sub> Huff and puff processes in Bakken formation. *Fuel* **2017**, *190*, 145–162. [[CrossRef](#)]
23. Zhou, X.; Li, X.; Shen, D.; Shi, L.; Zhang, Z.; Sun, X.; Jiang, Q. CO<sub>2</sub> huff-n-puff process to enhance heavy oil recovery and CO<sub>2</sub> storage: An integration study. *Energy* **2022**, *239*, 122003. [[CrossRef](#)]
24. Sheng, J. Optimization of huff-n-puff gas injection in shale oil reservoirs. *Petroleum* **2017**, *3*, 431–437. [[CrossRef](#)]
25. Monger, T.G.; Coma, J.M. Laboratory and field evaluation of the CO<sub>2</sub> huff ‘n’ puff process for light-oil recovery. *SPE Res. Eng.* **1988**, *3*, 1168–1176. [[CrossRef](#)]
26. Wang, Y.; Hu, J.; Xie, W.; Zhang, Y. Optimization and Analysis of CO<sub>2</sub> Huff-n-Puff Process in Shale Oil Reservoirs Using Response Surface Methodology (RSM). *Geofluids* **2022**, *2022*, 5927853. [[CrossRef](#)]
27. Hao, M.; Liao, S.; Yu, G.; Lei, X.; Tang, Y. Performance Optimization of CO<sub>2</sub> Huff-n-Puff for Multifractured Horizontal Wells in Tight Oil Reservoirs. *Geofluids* **2020**, *2020*, 8840384. [[CrossRef](#)]
28. Chen, C.; Balhoff, M.; Mohanty, K. Effect of Reservoir Heterogeneity on Primary Recovery and CO<sub>2</sub> Huff ‘n’ Puff Recovery in Shale-Oil Reservoirs. *SPE Res. Eval. Eng.* **2014**, *17*, 404–413. [[CrossRef](#)]
29. Zhong, H.; He, Y.; Yang, E.; Bi, Y.; Yang, T. Modeling of microflow during viscoelastic polymer flooding in heterogenous reservoirs of Daqing Oilfield. *J. Pet. Sci. Eng.* **2022**, *210*, 110091. [[CrossRef](#)]
30. Bui, D.; Nguyen, T.; Nguyen, T.; Yoo, H. Formation Damage Simulation of a Multi-fractured Horizontal Well in a Tight Gas/Shale Oil Formation. *J. Pet. Explor. Prod. Technol.* **2023**, *13*, 163–184. [[CrossRef](#)] [[PubMed](#)]
31. Dohmen, T.; Zhang, J.; Blangy, J.P. Measurement and Analysis of 3D Stress Shadowing Related to the Spacing of Hydraulic Fracturing in Unconventional Reservoirs. In Proceedings of the SPR Annual Technical Conference and Exhibition, Amsterdam, The Netherlands, 31 August 2014.
32. Dvory, N.Z.; Zoback, M.D. Prior Oil and Gas Production Can Limit the Occurrence of Injection-Induced Seismicity: A Case Study in the Delaware Basin Of Western Texas and Southeastern New Mexico, USA. *Geology* **2011**, *49*, 1198–1203. [[CrossRef](#)]
33. Hefner, W.; Davudov, D. Field Development Using Compositional Reservoir Simulation and Uncertainty Analysis in the Delaware Basin. In Proceedings of the SPE Oklahoma City Oil and Gas Symposium, Oklahoma City, OK, USA, 9 April 2019.



34. Bandis, S.C.; Lumsden, A.C.; Barton, N.R. Fundamentals of rock joint deformation. *Int. J. Rock Mech. Min. Sci. Geomech. Abstr.* **1983**, *20*, 249–268. [[CrossRef](#)]
35. Jarrell, P.M.; Fox, C.E.; Stein, M.H.; Webb, S.L. *Practical Aspects of CO<sub>2</sub> Flooding*; Society of Petroleum Engineers: Richardson, TX, USA, 2022; Volume 22.
36. Ginting, M.; Wijayanti, P.; Cindra, R.A. CO<sub>2</sub> MMP determination on L Reservoir by using CMG simulation and correlations. *J. Phys. Conf. Ser.* **2019**, *1402*, 055107. [[CrossRef](#)]
37. Lehmann, J.; Budge, J.; Palghat, A.; Petr, C.; Pyecroft, J. Expanding Interpretation of Interwell Connectivity and Reservoir Complexity through Pressure Hit Analysis and Microseismic Integration. In Proceedings of the SPE Hydraulic Fracturing Technology Conference and Exhibition, The Woodlands, TX, USA, 9–11 February 2016.
38. McKenna, J.; Grealy, M.; Blaz, M.; Toohey, N. Using depletion-zone microseismicity to understand producing volumes. In Proceedings of the SEG International Exposition and Annual Meeting, Dallas, TX, USA, 16–21 October 2016.
39. Khodabakhshnejad, A. Impact of Frac Hits on Production Performance—A Case Study in Marcellus Shale. In Proceedings of the SPE Western Regional Meeting, San Jose, CA, USA, 23–26 April 2019.
40. Gaswirth, S.B.; Marra, K.R.; Lillis, P.G.; Mercier, T.J.; Leathers-Miller, H.M.; Schenk, C.J.; Klett, T.R.; Le, P.A.; Tennyson, M.E.; Hawkins, S.J.; et al. Assessment of undiscovered continuous oil resources in the Wolfcamp shale of the Midland Basin, Permian Basin Province, Texas. *US Geol. Surv.* **2016**, 3092.
41. Nguyen, S.T.; Nguyen, T.C.; Yoo, H.; El-kaseeh, G. Geomechanical Study and Wellbore Stability Analysis for Potential CO<sub>2</sub> Storage into Devonian and Silurian Formations of Delaware Basin. In Proceedings of the SPE Oklahoma City Oil and Gas Symposium, Oklahoma City, OK, USA, 17–19 April 2023.
42. Energy Information Administration. *Permian Basin Part.1: Wolfcamp, Bone Spring, Delaware Shale Plays of the Delaware Basin*; US Energy Information Administration Report; US Energy Information Administration: Washington, DC, USA, 2020.
43. Bui, D.; Nguyen, S.; Nguyen, T.; Yoo, H. The Integration of Geomechanics and Reservoir Modeling for Hydraulic Fracturing and Well Spacing Optimization in the Third Bone Spring Sand of the Delaware Basin. In Proceedings of the SPE Eastern Regional Meeting, Wheeling, WV, USA, 3–5 October 2023.
44. Nguyen, S.T.; Hoang, S.K.; Khuc, G.H. Improved Pre-Drill Pore Pressure Prediction for HPHT Exploration Well Using 3D Basin Modeling Approach, a Case Study Offshore Vietnam. In Proceedings of the Offshore Technology Conference Asia, Kuala Lumpur, Malaysia, 20–23 March 2018. Paper SPE-28606-MS.
45. Snee, J.L.; Zoback, M.D. State of Stress in the Permian Basin, Texas and New Mexico: Implications for Induced Seismicity. *Lead. Edge* **2018**, *37*, 127–134. [[CrossRef](#)]
46. Ojha, S.P.; Misra, S.; Tinni, A.; Sondergeld, C.; Rai, C. Relative permeability estimates for Wolfcamp and Eagle Ford shale samples from oil, gas and condensate windows using adsorption-desorption measurements. *Fuel* **2017**, *208*, 52–64. [[CrossRef](#)]
47. You, J.; Ampomah, W.; Morgan, A.; Sun, Q.; Huang, X. A comprehensive techno-economic assessment of CO<sub>2</sub> enhanced oil recovery projects using a machine-learning assisted workflow. *Int. J. Greenh. Gas Control.* **2021**, *111*, 1750–5836. [[CrossRef](#)]

**Disclaimer/Publisher’s Note:** The statements, opinions and data contained in all publications are solely those of the individual author(s) and contributor(s) and not of MDPI and/or the editor(s). MDPI and/or the editor(s) disclaim responsibility for any injury to people or property resulting from any ideas, methods, instructions or products referred to in the content.